Earth's Future

RESEARCH ARTICLE
10.1029/2024EF005078

Physics-Based Hazard Assessment of Compound Flooding From Tropical and Extratropical Cyclones in a Warming Climate

Ali Sarhadi[1,2], **Raphaël Rousseau-Rizzi**[1], **and Kerry Emanuel**[1]

[1]Lorenz Center, Department of Earth, Atmospheric, and Planetary Sciences, Massachusetts Institute of Technology, Cambridge, MA, USA, [2]School of Earth and Atmospheric Sciences, Georgia Institute of Technology, Atlanta, GA, USA

Key Points:

- A newly developed model simulates the interplay of surge and rainfall flooding from tropical and extratropical cyclones in a warming climate
- Tropical cyclone-induced compound flooding hazard increases with evolving storm climatology and rising sea levels in a warming climate
- Extratropical cyclone-induced flooding increases in coastal areas with sea-level rise, while staying minimal inland in a warming climate

Supporting Information:

Supporting Information may be found in the online version of this article.

Correspondence to:

A. Sarhadi,
sarhadi@mit.edu

Citation:

Sarhadi, A., Rousseau-Rizzi, R., & Emanuel, K. (2025). Physics-based hazard assessment of compound flooding from tropical and extratropical cyclones in a warming climate. *Earth's Future*, *13*, e2024EF005078. https://doi.org/10.1029/2024EF005078

Received 9 JUL 2024
Accepted 28 OCT 2024

Abstract Recent efforts to assess coastal compound surge and rainfall-driven flooding hazard from tropical (TCs) and extratropical cyclones (ETCs) in a warming climate have intensified. However, challenges persist in gaining actionable insights into the changing magnitude and spatial variability of these hazards. We employ a physics-based hydrodynamic framework to numerically simulate compound flooding from TCs and ETCs in both current and future climates, focusing on the western side of Buzzards Bay in Massachusetts. Our approach leverages hydrodynamic models driven by extensive sets of synthetic TCs downscaled from CMIP6 climate models. We also perform a far less extensive analysis of ETCs using a previously produced event set, dynamically downscaled using the WRF model driven by a single CMIP5 model. This methodology quantifies how climate change may reshape the compound flooding hazard landscape in the study area. Our findings reveal a significant increase in TC-induced compound flooding hazard due to evolving climatology and sea level rise (SLR). Although compound flooding induced by ETCs increases mostly in coastal areas due to SLR, inland areas exhibit almost no change, and some even show a decline in rainfall-driven flooding from high-frequency ETC events toward the end of the century compared to the current climate. Our methodology is transferable to vulnerable coastal regions, serving as a tool for adaptive measures in populated areas. It equips decision-makers and stakeholders with the means to mitigate the destructive impacts of compound flooding arising from both current and future TCs, and shows how the same methodology might be applied to ETCs.

Plain Language Summary During storms in coastal areas, strong winds can cause surge-driven flooding, and simultaneously, intense rainfall may lead to inland heavy rainfall-driven flooding. Sometimes, these two flooding sources coincide, forming compound surge- and rainfall-driven flooding, which is more destructive than either hazard alone. To assess the hazard of such destructive compound flooding, we use physics-based models to quantify the frequency and magnitude of these hazards. Additionally, we evaluate how climate change and factors such as SLR may affect the frequency and magnitude of such events in coastal areas. Through these detailed and granular hazard assessments, regions facing increased flooding threats can develop strategies to more effectively mitigate damages posed by compound flooding during extreme storms.

1. Introduction

Tropical cyclones (TCs) are powerful storms characterized by strong winds, heavy precipitation, and storm surges. They predominantly affect tropical coastal areas, where they can cause significant annual damage, estimated at US$26 billion in the United States alone (Bakkensen & Mendelsohn, 2019). However, recent scientific evidence indicates a notable poleward shift in TC distribution. This shift is attributed in part to global climate warming and ocean temperature rise, which create conducive conditions for the formation and propagation of TCs into higher latitudes (Kossin, 2018; Kossin et al., 2014). As TCs extend into higher latitudes, they introduce new challenges and hazards. These areas are less accustomed to such extreme weather events, and their populations, infrastructure, and ecosystems may be poorly prepared to cope with them (Studholme et al., 2022). In addition to TCs, which occur during warm seasons, extratropical cyclones (ETCs) develop during cold seasons in these regions. ETCs can experience slower movement as a result of atmospheric conditions, leading to an elevated likelihood of causing substantial damage (Booth et al., 2021; Colle et al., 2015).

Damage resulting from TCs and ETCs is associated with various hazards inherent to these weather systems. Strong winds and low pressure accompanying these storms during landfall can induce storm surges in coastal regions, leading to coastal flooding. Heavy rainfall can result in inland freshwater flooding. At times, both forms

of flooding can occur simultaneously, resulting in a compound event that combines storm surge and rainfall-driven flooding. The intricate interplay between these two sources of flooding often results in compound flooding events that exhibit greater destructive potential compared to individual occurrences of either surge or rainfall-driven flooding (Wahl et al., 2015).

In a warming climate, several factors may contribute to changing potential for compound flooding events resulting from TCs and ETCs. It is well-established that the intensity of rainfall associated with these storms is likely to increase. This escalation is primarily driven by higher saturation vapor pressure of water, as dictated by the Clausius-Clapeyron equation (Liu et al., 2019). Furthermore, the movement of TCs toward higher latitudes, alterations in their translational speed, and modifications in the behavior of ETCs all contribute to the altered hazards associated with these storms (Booth et al., 2021; Kossin, 2018). Additionally, rising sea levels further exacerbate the impact of compound flooding events, necessitating a comprehensive evaluation and mitigation of the associated hazard (Lin et al., 2016, 2019; Marsooli et al., 2019; Strauss et al., 2021). It is important to gain a deeper understanding of how these alterations in storm characteristics, manifesting within a warming climate, may reshape the hazard of compound flooding resulting from these storms. This is particularly vital in regions unaccustomed to such cyclonic activity, as this knowledge is essential for enhancing preparedness, facilitating adaptation, and formulating mitigation strategies aimed at reducing the potentially devastating damages and casualties associated with these events.

One significant challenge associated with TCs is the limited availability of comprehensive historical records of these storms. The most reliable records we can obtain date back only to the early satellite era, starting in the 1980s. However, for ETCs, reanalysis data provide more extensive historical records, likely reliable back to 1900. This extended data set allows for a more robust analysis of trends and patterns over a longer period for ETCs. The timeframe for reliable TC data set is relatively short, and for specific regions, some landfalling storms may not have been recorded, exacerbating the issue. Consequently, when attempting to employ historical records to quantify the hazard of compound flooding from these storms, a significant degree of uncertainty arises due to the brevity of the data set and the paucity of observations. Even if more extended records of these storms were available from the past, they may not be representative of today's climate, primarily due to the influence of climate change. It is important to emphasize that even contemporary climate records do not provide an accurate representation of future conditions, again owing to ongoing climate change. Therefore, any statistical risk assessment method relying solely on historical statistics may fail to accurately quantify the hazard. Infrastructure or adaptation planning based on such methodologies can thus lead to vulnerabilities and significant damages. To address this data limitation and account for the evolving climate, we employ a physics-based hazard modeling framework (Sarhadi et al., 2024). This framework is driven by the atmospheric and ocean climatology of reanalysis data and General Circulation Models (GCMs) (Emanuel et al., 2006, 2008; Komurcu et al., 2018). It enables the downscaling of TCs and ETCs across past, current, and future climate scenarios. This approach helps address the dearth of observations and provides insights into how these storms may evolve under a warming climate, consequently shedding light on how the hazard of compound flooding in coastal areas at higher latitudes may change. Here, the term hazard is used to denote the statistical frequency of flood events as characterized by their return periods, which correspond to the inverse of the annual exceedance probability.

Compound flooding arises from the complex interplay between storm surge- and heavy rainfall-driven inundation, manifesting across both spatial and temporal dimensions. It is important to meticulously model this intricate hydrodynamic interaction between the two sources of flooding, distinguished by their surge and rainfall characteristics, with a high level of temporal and spatial precision. In recent years, there has been a growing focus on modeling intricate coastal hydrodynamics. Commonly, statistical methodologies are used to assess flood hazard by establishing joint statistical distributions that capture interdependencies among various flooding drivers, often at localized or gauge scales (Gori & Lin, 2022; Gori et al., 2020; Moftakhari et al., 2017; Wahl et al., 2015; Zhang & Najafi, 2020). However, these methods have limitations, primarily stemming from their inability to account for the complex dynamic interactions between storm surge and rainfall-driven flooding. These approaches rely heavily on statistical measures of dependence, which can introduce uncertainties. Moreover, they often overlook the hydraulic dynamics of compound flooding, which involve integrating surge height and rainfall intensity to determine flooding levels while accounting for their compounded effects. The prevailing statistical practices, which often treat the drivers of compound flooding (rainfall intensity and surge height) through joint distributions rather than accounting for the actual hydraulically driven flooding, result in imprecise compound flooding hazard and risk assessments. Numerous studies have explored coastal flooding stemming from TCs and ETCs through

the utilization of physics-based modeling methodologies (Emanuel, 2017; Gori et al., 2020; Lin et al., 2019; Marsooli et al., 2019). However, the majority of these studies have primarily focused on single hazard scenarios, such as rainfall- or surge-induced flooding, or on combining separate hazards. Therefore, these approaches may underestimate or overestimate flooding hazard frequency compared to models that account for the hydrodynamics of compound flooding. In our study, we employ an innovative approach designed to overcome the limitations often associated with these conventional methodologies. Our method utilizes a physically based numerical hydrodynamic model, allowing for the explicit simulation of compound flooding. This is accomplished by concurrently converting key driving factors, such as wind speed and rainfall intensity, into hydraulic-based flood simulations, providing a high level of temporal and spatial resolution to comprehensively capture the complex interplay between surge and rainfall-driven flooding during the landfall of TC or ETC storms.

By utilizing a state-of-the-art data set of downscaled storms, combined with an understanding of the climatology of these storms and projected SLR in the current and future warming climate, we can evaluate the potential evolution of compound flooding hazard in coastal areas. This approach also allows us to identify the primary drivers that may intensify the hazard of compound flooding. Such information can provide a detailed granular perspective on the risk of compound flooding in coastal regions, enabling authorities to enhance their preparedness and adaptation strategies for coastal cities and communities. This proactive approach is crucial for mitigating damages in the current and future climates.

2. Data Set and Methodology

2.1. Synthetic Tropical Cyclone Model and Data Sets

To comprehensively address the multiple hazards associated with TCs, we begin by creating synthetic TC events using the methodology detailed in Emanuel et al. (2006, 2008). This method employs deterministic and numerical downscaling to generate synthetic TCs by introducing random seeding in both spatial and temporal dimensions across the entire Atlantic Ocean basin. The initial wind intensity of these seeded TCs is determined through a deterministic calculation, utilizing a high-resolution, coupled ocean-atmosphere TC model. This model is driven by the thermodynamic conditions of the ocean and atmosphere, taking into account various factors, including monthly mean sea surface temperature, atmospheric temperature, humidity, and daily interpolated horizontal winds at altitudes of 250 and 850 hPa (Emanuel et al., 2008).

It's important to note that any storms failing to intensify to wind speeds exceeding 21 m/s (equivalent to 40 knots) are excluded from the data set. In a natural selection process, only seed vortices encountering favorable large-scale environmental conditions intensify into TCs, with their development timing synchronized with environmental climatic patterns. The intensity of TCs is determined using the Coupled Hurricane Intensity Prediction System (CHIPS), which is an axisymmetric hurricane model coupled to a 1D ocean model (Emanuel et al., 2004). For the purposes of this study, we fix the initial condition of the TC outer radius at 400 km, however, apart from this, the structure of the vortex, including the radius of maximum winds, evolves by the model physics. The dynamic downscaling method enables the simulation of numerous synthetic TC events, driven by bias-corrected climate reanalysis data or projections from CMIP6 GCMs. Throughout the entire lifespan of each synthetic TC, we consistently record key meteorological parameters, including maximum surface wind speed, central pressure, and the radius of maximum winds. These parameters are saved at 2-hr intervals. Subsequently, a hydrodynamic model known as GeoClaw (Mandli & Dawson, 2014) is used to simulate wind-induced storm surges with high temporal resolution along the coastline near the study area during the landfall of each synthetic TC (further details on this modeling process can be found in the provided reference).

In addition to generating primary drivers for storm surges from synthetic TCs, we also produce high-resolution hourly rainfall intensity data at a spatial resolution of approximately 20 m for the vicinity of the study area during the landfall of each synthetic TC using a Tropical Cyclone Rainfall (TCR) model (Feldmann et al., 2019). TCR, a physics-driven model, links convective rainfall in TCs to the TC vortex's vertical velocity, accounting for factors such as frictional convergence, topography, vortex stretching, baroclinic effects, and radiative cooling. Previous studies have applied TCR in hazard frequency assessments (Emanuel, 2017; Gori & Lin, 2022) and validated it against observed TC-related rainfall in the United States (Feldmann et al., 2019; Xi et al., 2020). These studies demonstrated TCR's accuracy in replicating coastal rainfall patterns but noted limitations in inland and mountainous areas. To assess the accuracy of this rainfall data set, Feldmann et al. (2019) conducted an evaluation by comparing it with observed rainfall data obtained from the NEXRAD radar network and rain gauges across the

eastern United States. This high-resolution, hourly rainfall intensity data plays a critical role in quantifying the rainfall-induced hazard, a key component of the compound flooding process.

The downscaling process is implemented for six distinct CMIP6 climate model simulations: CESM2, CNRM-ESM2-1, EC-EARTH3, IPSL-CM6A-LR, MIROC6, and UKESM1-0-LL, all operating under the SSP3-7.0 scenario. Synthetic TC tracks are generated for two different time periods: the late 20th century, spanning 1971–2000, and the end of the century, from 2071 to 2100, using the climate model simulations. The entire data set comprises approximately 46,800 synthetic storms, with about 3,900 synthetic storms generated from each climate model in each period. Furthermore, we repeat this process to generate 4,100 synthetic storms based on NCEP reanalysis data, representing the late 20th century (1979–1999) and current climates (2000–2020). In total, these data sets encompass a large set of synthetic TCs, with their centers passing within 300 km of the New Bedford city in the study area. The TC downscaling technique described here accounts for some features of extratropical transition. Namely, the effects of increasing background flow and shear can contribute substantially to surface winds generated by the technique. On the other hand, there can be no feedback of the TC back onto the environmental flow, except indirectly as entailed in the beta-drift component of storm translation. Some, and perhaps most, of our synthetic TC events might be considered by forecasters to be undergoing extratropical transition by the time they affect Buzzards Bay, Massachusetts. We here make no attempt to distinguish between such events and other events more nearly resembling classical TCs. Later, when we consider ETCs, we will attempt to exclude TCs by confining our attention to the colder months of the year.

2.2. Extratropical Cyclone Data Sets

The method described above, which involves statistically and deterministically downscaling TCs, enables the simulation of a vast number of idealized synthetic TC events based on climate reanalysis or climate model simulations (Emanuel et al., 2008). This is possible, to a reasonable extent, because the feedback of TCs on the surrounding large-scale environment does not significantly impact their subsequent evolution. For example, TC tracks are primarily determined by the large-scale flow in which they are embedded (and, to a lesser extent, by the beta drift effect), which passively advects them (Emanuel et al., 2006), irrespective of the TCs' internal evolution. Additionally, this method employs analytical simplifications, such as assuming axisymmetry and moist slantwise-neutrality in the free troposphere, which reduces the downscaling model to a single radial dimension, making it computationally efficient, even at high radial resolution.

However, for ETC events, it is not feasible to neglect the effects of the storm on the large-scale environment. Therefore, it is not possible to generate additional synthetic ETCs within a given global climate model run. Only storms explicitly simulated in these runs can be dynamically downscaled. At present, there are no reduced-dimension models that can be used to dynamically downscale ETCs, so computationally expensive regional climate models like the Weather Research and Forecasting (WRF) model (Komurcu et al., 2018) are required to provide high-resolution information on the behavior of ETCs for hazard frequency assessment. Due to the difficulty and computational cost associated with simulating a large number of downscaled ETC events, we do not attempt to do this ourselves. Instead, we utilize state-of-the-art WRF dynamical downscaling data described in Komurcu et al. (2018). These downscaling simulations were developed to support regional climate studies in the northeastern U.S. They downscale CMIP5, RCP8.5 projections by CESM v1.0, which have been bias-corrected to support climate research. The WRF data used here cover two different time periods: the 2006–2020 current climate period and the 2081–2100 end-of-the-century period, with hourly time resolution. Additionally, we used the output of a 2006–2015 WRF simulation to downscale ERA-Interim reanalysis data (Dee et al., 2011), which aided in verifying our model. The WRF simulations employ nested domains on a Cartesian grid, with the innermost domain covering 1,500 km by 1,200 km and using uniform convection-permitting 3 km resolution. To simulate rainwater flooding and storm surge in the study area, we require downscaled precipitation rates, surface pressure, and surface winds, which must be transformed from the WRF Lambert conformal conic projection to the geographical coordinates used in the hydraulic and surge models. More detailed information can be found in Sarhadi et al. (2024).

To assess the hazard associated with compound flooding, we compile a catalog of potential freshwater and surge flooding events linked to ETCs for each downscaled period. To identify potential freshwater flooding events, we calculate time series of rainfall intensity averaged over the area extending from −71.2 to −70.5 W and 41.5–41.9 N for each historical and future period. Potential freshwater flooding events are selected iteratively. The

process involves searching for rainfall intensity maxima in the time series in decreasing order, starting from the global maximum. Each event extends from 4 days before to one day after the selected local maximum. Once an event is defined, its full time-span is removed from the time series so that the next, slightly weaker event selected is the most intense remaining event in the time series. The total number of events selected in each downscaled period is equal to five times the number of years in the corresponding period. Similarly, to identify potential surge flooding events, we select maxima in a time series of the wind component oriented toward the coast averaged over a $2° \times 2°$ box off the coast of the western Buzzards Bay area. It is important to note that the instantaneous precipitation intensity averaged over the study area and the average wind component oriented toward the coast are only rough predictors of freshwater and storm surge flooding. However, the number of selected rainfall and wind events is sufficient to ensure that all events capable of producing significant freshwater or surge flooding are included. To minimize the inclusion of TCs, our focus is on ETC events occurring from October to May. However, we acknowledge the potential for some overlap between TCs and ETCs in early October. Differentiating ETCs from extratropical-transitioned TCs in dynamically downscaled simulations requires nuanced understanding of atmospheric dynamics and storm structure. This area necessitates further exploration in future studies.

2.3. Storm Surge Modeling

Consistent with previous research (A. J. Garner et al., 2017; Lin et al., 2016; Reed et al., 2015), we define a storm surge as the anomalous elevation of sea level above Relative Sea Level (RSL). This elevation results from the low atmospheric surface pressure and the high surface wind speed associated with TCs or ETCs. The combination of storm surge and RSL fluctuations characterizes the surge height in coastal regions caused by TCs and ETCs. Our RSL estimation is based on the local average of the total sea level throughout each climate period. RSL also serves as the key factor for distinguishing between land and water elevations. As a result, we disregard interannual sea level variations and the relatively minor nonlinear interactions between the surge and RSL, as outlined in prior studies (Lin et al., 2016). Furthermore, astronomical tides are not factored into our calculations. It is important to note that future studies should investigate the effects of tides and their nonlinear interactions with surges, particularly in light of potential changes due to SLR (A. J. Garner et al., 2017; Müller, 2011).

To simulate storm surges generated by synthetic TCs and ETCs, we utilize the GeoClaw numerical model, which relies on high-resolution shock-capturing finite volume methods. GeoClaw utilizes the classical shallow-water equations, enhanced with additional source terms to accommodate various physical processes, such as bathymetry effects, bottom friction, wind friction, non-constant surface pressure, and Coriolis forcing. Further details on the numerical modeling approach can be found in Mandli and Dawson (2014). Unlike finite-element unstructured hydrodynamic models (Colle et al., 2008; Westerink et al., 2008), GeoClaw incorporates Adaptive Mesh Refinement (AMR) algorithms (Berger et al., 2011; Mandli & Dawson, 2014), enabling efficient computational solutions at high resolutions over large scales. We implement a broad domain, covering approximately 1,000 km, to better quantify the large-scale impact of various attributes of TCs and ETCs, including intensity, duration, size, and landfall location, on storm surges. GeoClaw, which utilizes the Holland wind field model to compute near-surface winds based on parameters such as eye location, radius of maximum winds, maximum wind speed (V_{max}), and central pressure, falls short in accurately capturing the wind fields of ETCs, whose wind fields are highly asymmetric. This inadequacy impacts the representation of storm surges in GeoClaw. Given that the GeoClaw model is specifically designed for TCs, applying it to ETCs leads to significant inaccuracies. To rectify this, it is essential to bypass the Holland model and instead directly incorporate wind fields and surface pressure fields derived from WRF simulation data into GeoClaw. This adaptation requires modifications to the model to better reflect the unique characteristics of ETCs and enhance the accuracy of storm surge simulations. These changes also expand GeoClaw's applicability to a broader range of cyclonic events.

In our study area along the coastline, we positioned synthetic gauges at intervals of approximately 20 m to ensure comprehensive spatial coverage. This spacing was chosen with considering for the complexity of the coastline and the desired level of detail. The selection of optimal spatial resolution was based on the need to accurately capture intricate interactions between storm surges from TCs and ETCs and land features, while also ensuring computational feasibility for analyzing a large data set of events. Consequently, these coastal surge conditions are transformed into surge-driven flooding through a hydraulic model, allowing us to model the propagation of surges and their potential to cause surge-driven flooding in coastal areas. Furthermore, temporal resolution is less than a minute during landfall to enhance our simulation of the dynamic interaction between surge and rainfall-driven

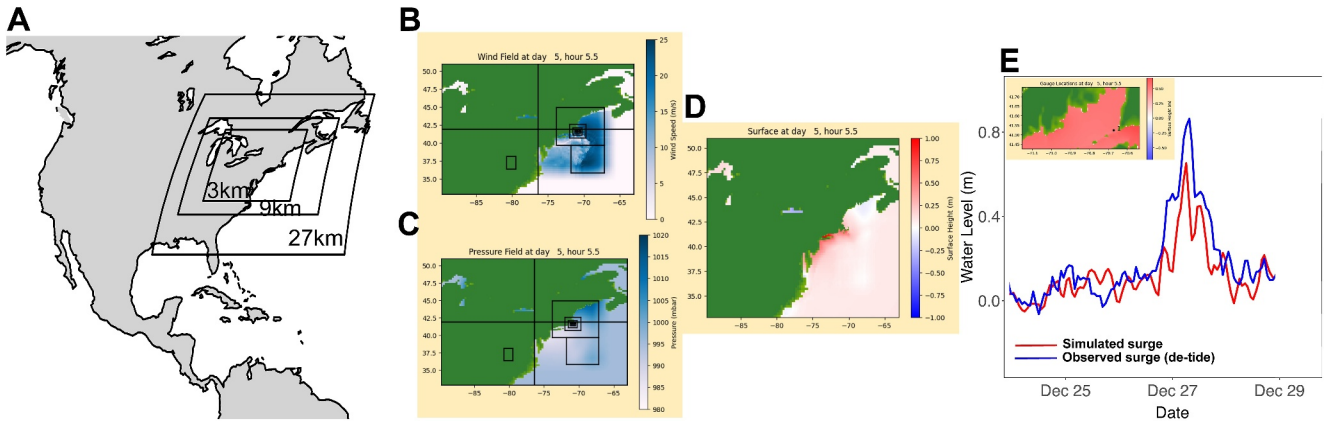

Figure 1. Surge simulation process for ETCs using dynamically downscaled WRF simulations of primary drivers (wind speed and sea level pressure fields) in the study area and performance evaluation (a) Three nested grids with spatial resolutions of 27, 9, and 3-km used for dynamically downscaling WRF simulations (in this study, we focus on the 3-km spatial resolution domain). (b and c) Hourly wind and pressure fields downscaled via WRF simulations driven by ERA-Interim reanalysis for an ETC event that occurred on 27–28 December 2012. (d) Simulated surge height (in meters) from the ETC at the regional scale, using modified GeoClaw. (e) Performance evaluation of GeoClaw for the ETC storm. The blue line represents observed surge heights during the landfall of the ETCs, calculated by de-tiding water levels, with water elevation subtracted from NOAA tide predictions at the Woods Hole gauge. The red line represents surge heights simulated by GeoClaw. Note that the temporal resolution on the *x*-axis is 6 min.

flooding. This surge simulation approach is applied to a broad set of synthetic TC and ETC events. It is worth noting that while the performance of GeoClaw in modeling TC surges has been evaluated in previous studies (Mandli & Dawson, 2014; Miura et al., 2021; Sarhadi et al., 2024), here we rigorously calibrated the GeoClaw model for the Buzzards Bay area, focusing specifically on adjusting the bottom friction coefficients and coastal features. The model's storm surge simulations were then evaluated against observed surge events recorded at the Woods Hole gauge. This evaluation process ensures that our model accurately reflects the local hydrodynamic conditions, providing reliable storm surge simulations for the area as discussed presently.

While the accuracy of dynamically downscaled ETCs was evaluated in a previous study (Komurcu et al., 2018), here, we utilize the downscaled ETCs to assess their performance in surge modeling. Figure 1 illustrates the surge modeling process, which entails dynamically downscaled WRF simulations of primary surge drivers, including wind and pressure fields, forced by ERA-Interim reanalysis data. The simulation corresponds to an historical ETC event that occurred on 27–28 December 2012, within the study area. The calibrated model's performance accuracy is depicted in Figure 1. Further details on the calibration process of the GeoClaw model, including specific parameter adjustments and their impacts on simulation outcomes, are provided in Figure S1 of the Supporting Information S1. The simulated surge, using the modified GeoClaw model, demonstrates a robust agreement with observed surge levels. These observed surge values were obtained by de-tiding water levels, a procedure that involves subtracting water elevation from NOAA tide predictions at the Woods Hole gauge.

For modeling surges generated by TCs and ETCs during the late 20th century and in the current climate, we rely on RSL data obtained from NOAA gauge observations. However, in the context of future climate scenarios, we incorporate SLR projections derived from CMIP6 under the SSP3-7.0 scenario into GeoClaw using a "bathtub" approach. The bathtub approach treats the water body as a static entity, where the sea level rises uniformly, akin to water filling a bathtub without any waves or currents. This approach calculates flood depths by modeling the impact of elevated water levels over complex topographical features (Kasmalkar et al., 2024; Shepard et al., 2012). Due to its simplicity, the bathtub approach is easier and faster to apply in predictive SLR modeling within hydrodynamic contexts and requires less computational power. We integrate this approach into the GeoClaw model, where we incorporate elevated water levels (from projected SLR) across the entire computational domain. This adjustment enables the hydrodynamic model to simulate storm surge along the coastline with these elevated sea levels. This integration allows us to assess the effects of rising sea levels on compound flood inundation caused by TCs and ETCs, as well as their associated hazard landscape under current and future climates. This approach provides a robust framework to quantify the evolving hazards of storm surges and compound flooding due to SLR. Future projected sea levels involve the ensemble mean of total SLR over future climate scenarios (Fox-Kemper et al., 2021). These projections encompass comprehensive considerations,

including the contributions of Antarctic and Greenland ice sheets, glacier dynamics, thermal expansion of seawater, terrestrial water storage, vertical land motion, and the potential influences of marine ice cliff instability.

2.4. Numerical Compound Flood Modeling

Compound flooding arises from the confluence of storm surge and heavy rainfall-driven flooding caused by synthetic TCs and ETC events. To simulate the complex hydrodynamic interactions involved in compound flooding, we modified a version of the LISFLOOD-FP model. This two-dimensional hydraulic model, renowned for its high spatio-temporal resolution, is recognized for its computational efficiency. The two-dimensional base model employs an explicit forward difference scheme on a staggered grid. The model is structured around two fundamental hydrodynamic equations: the continuity equation, which ensures mass conservation within each computational cell, and the momentum equation, which governs the flow dynamics between cells. This setup allows for the accurate simulation of fluid motion and mass transport in hydrological contexts. A detailed description of this model is provided in Neal et al. (2012). LISFLOOD-FP employs an explicit finite difference scheme to simulate shallow water waves, while deliberately omitting advection (Bates et al., 2010). The efficacy of the fundamental model's numerical scheme in simulating pluvial and fluvial flood dynamics has been substantiated by various studies (Bates et al., 2021; Neal et al., 2012; Wing et al., 2022). In our work, this model has been customized to incorporate high-resolution surge height data (simulated by GeoClaw) along the coastline, and simultaneously, it accommodates hourly rainfall intensity data from storm events in the inland regions as boundary conditions. In our simulations, the spatial resolution is approximately 20 m, matching the resolution of the Digital Elevation Model (DEM) used. We conduct simulations at high temporal resolutions, less than a minute, similar to storm surge simulations, and perform mass conservation checks every 20 min. These frequent checks help maintain numerical accuracy in mass flow and storage calculations throughout the simulation. This physically based approach empowers the model to replicate the dynamics of compound flooding in response to the rapid spatio-temporal fluctuations in surge and rainfall driven flooding during the landfall of each storm. The model ensures the conservation of mass within each grid cell and maintains momentum continuity between neighboring cells. The model recalculates the flow depth, taking into account the elevation of each cell, water surface slope, surface Manning's roughness coefficient, and acceleration due to gravity. More details about the methodology can be found in Sarhadi et al. (2024).

It is important to note that the geodetic datum of NAD83 is utilized to establish the spatial coordinates, while the vertical datum of NAVD88 is used for elevation values within the applied DEM. In our study, we utilize a LiDAR-based DEM, employing a geographic (Lat/Lon) projection to represent the area's geometry. The land-use of the study area, derived from the National Land Cover Dataset (Dewitz, 2021), is employed to quantify surface roughness. The surface roughness coefficients are estimated for each land use class (Kalyanapu et al., 2009). These coefficients range from 0.0113 to 0.40. Figure S2 in Supporting Information S1 illustrates the spatial distribution of surface roughness within the study area. A map of available soil water storage for the topsoil layer (0–50 cm) with the same spatial resolution is used to account for the infiltration rate in non-constructed and constructed areas (Figure S2 in Supporting Information S1). The source of these input files is given in Data Availability Statement.

In addition to evaluating surge modeling discussed in the previous section, we also assessed the accuracy of the LISFLOOD-FP model for simulating rainfall-driven flooding in inland areas during the same ETC event in 2012. This evaluation used calibrated input parameters, including the Manning coefficient and infiltration rates. Figure S3 in Supporting Information S1 illustrates the model calibration process, highlighting the effects of varying these parameters on the simulated flood levels at a USGS gauging station. The results indicate that the calibrated model successfully replicates both the peak flood level and the timing of the flood's peak, closely aligning with the observed data during the event.

In the hydrodynamic modeling process, compound flooding during the landfall of each storm is simulated in detail, capturing all relevant physical interactions and dynamics with high temporal and spatial resolution. We then store the maximum compound flooding level at each grid cell for every individual storm event. This process is iteratively conducted for a vast set of TCs and ETCs derived from reanalysis and climate models. These maximum flood records serve as a reflection of the compound flooding behavior over each defined time period for every grid cell. Subsequently, these records are fundamental in constructing a nonparametric empirical

Cumulative Distribution Function (eCDF). This approach leverages the theory of nonexceedance probability to determine the return period of a compound flooding event at each grid cell. The calculation is expressed as:

$$T_H(h) = \frac{1}{P(H > h)} \quad (1)$$

In this equation, $P(H > h)$ signifies the annual probability that the compound flooding level of an event (H) exceeds a specific threshold (h), and $T_H(h)$ corresponds to the return period of that particular event. The ensemble mean of compound flooding levels for TCs and ETCs at various return periods is then computed by considering multiple climate models across distinct time periods. The assessment of expected changes in compound flooding levels at specific return periods is carried out by evaluating the disparities between the ensemble mean of flood levels in future climate scenarios and those in past or current climate conditions. To dissect the individual and collective influences of changes in storm climatology and SLR on the granular hazard of compound flooding, our approach involves running the hydraulic model twice for each individual storm. This includes one simulation with the incorporation of SLR and another without it. Running the hydraulic model twice—once with SLR and once without—allows us to discern and quantify the distinct and synergistic effects of variations in storm climatology and SLR on the hazard of compound flooding. To distinguish the contribution of each individual hazard (surge or rainfall-driven flooding) in compound flooding from each storm, we can simply run the model with only one driver as the boundary condition.

3. Results and Discussion

3.1. Impact of Primary Driver Severity on Compound Flooding

Here, we evaluate the influence of the primary drivers during the landfall of TCs on the magnitude and extent of inundation associated with compound flooding in the study area. This assessment is pivotal for understanding the complexities of flood hazards caused by these meteorological phenomena. High wind speeds and low atmospheric pressure during the landfall of TCs lead to storm surge-driven flooding along coastal regions. Specifically, the greater the wind speed, the more intense and higher the storm surge becomes both before and during landfall. Concurrently, high rainfall intensity during landfall contributes to rainfall-driven flooding. The interplay between these flooding hazards, as analyzed in this study, explains the mechanisms driving the devastating impacts of compound flooding caused by TCs. The dominance of each primary driver determines the severity of the compound flooding hazard. Depending on which primary driver predominates, it may result in scenarios such as compound flooding with a dominant surge in coastal areas, a situation where rainfall-driven flooding in inland areas is more pronounced, or instances when both drivers are strong, leading to a severe compound flooding event characterized by both surge and rainfall-driven inundation.

By examining the primary drivers, our study offers essential insights into the dynamics of compound flooding, including the magnitude and extent of inundation. To illustrate this, we selected two TCs as case studies to demonstrate how the magnitude of primary drivers can affect the resulting compound flooding. Figure 2 (top panels) presents information on the primary drivers of these two synthetic TC storms, which were derived from downscaling NCEP reanalysis data for the current climate (2000–2020). These measurements are presented before and during landfall.

In the first case, represented by synthetic track #1337 (Figures 2a and 2b), the primary drivers include strong wind speeds at the eye of the TC before and during landfall. Rainfall intensity reaches up to 90–120 mm/hr in certain grid cells, with an average wind speed of 40 knots. The duration of high wind speeds is also an important factor to consider. These primary drivers result in flooding depths of up to 3 m in some low-land coastal and inland areas. In contrast, the second case, depicted by synthetic track #1339 (Figures 2c and 2d), exhibits lower rainfall intensity, with the upper tail reaching up to 10 mm/hr, and wind speeds at the eye barely reaching 40 knots in the upper tail. These conditions result in significantly lower flooding levels, particularly in inland areas, due to reduced rainfall intensity. Additionally, the spatial extent and magnitude of compound flooding in coastal areas are diminished compared to the first case, attributable to lower wind speeds and rainfall intensity.

This understanding offers a comprehensive and scientifically robust exploration of the relationship between the magnitude of primary drivers—specifically, rainfall intensity and surface wind speed—and the resulting complex

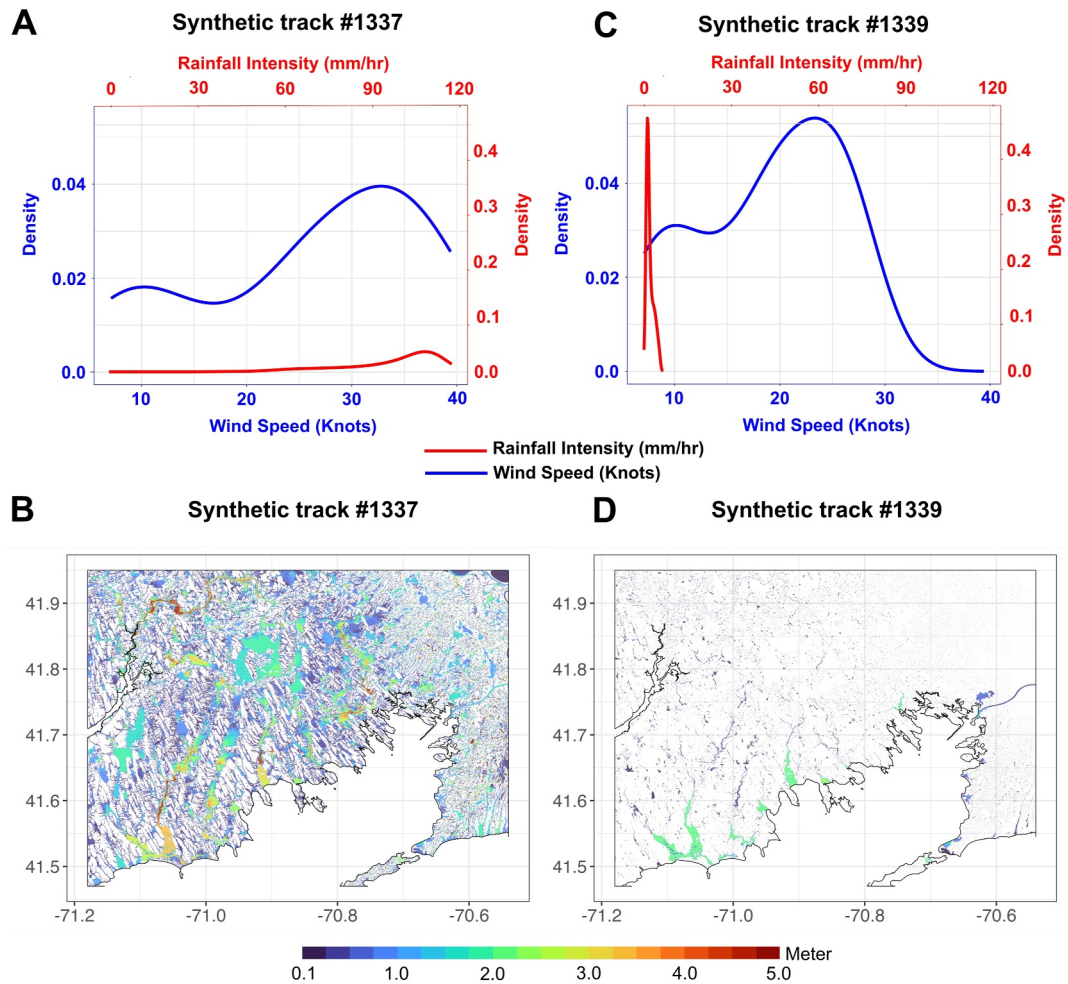

Figure 2. Impact of key drivers of compound flooding, such as rainfall intensity and surface wind speed. The top panels include the Probability Distribution Function of rainfall intensity (mm/hr) at each grid cell during landfall and the maximum surface wind speed (knots) at the eye of synthetic TC tracks, both before and at the time of landfall, for two selected synthetic TCs in the current climate downscaled by NCEP reanalysis data. The lower panels depict the corresponding compound flooding response for the two synthetic TCs. Panels (a and b) show the drivers and compound flooding for TC track #1337, while (c and d) show the same results for synthetic TC track #1339.

dynamics of compound flooding. These insights are invaluable for advancing our understanding of the multi-faceted flood hazards associated with TCs, which, in turn, contribute to a more informed and resilient approach to disaster preparedness. Using this approach, one can easily quantify the proportion of each individual hazard and analyze the dynamic interplay between them in generating compound flooding, with high temporal and spatial resolution. Notably, the same methodology can be readily applied to ETC storms. This deeper understanding improves forecasting, risk assessment, and preparedness in vulnerable coastal regions, enhancing resilience against storm impacts. In the subsequent section, we explain the contribution of each individual and compound hazard to the hazard frequency assessment and emphasize the significance of a physics-based approach to compound flooding.

3.2. Assessing the Effect of Tropical Cyclone Compound Flooding

In this section, we present a comparative analysis of compound flooding, delineating the individual contributions of surge and rainfall-driven flooding with a focus on coastal areas. The objective is to clarify the effects and potential hazards of compound flooding. Additionally, we examine how other approaches, such as singular hazards, surge, and rainfall-driven flooding considered individually, or a linearly additive hazards approach, may lead to the underestimation or overestimation of the hazard frequency. It is important to note that our

10.1029/2024EF005078

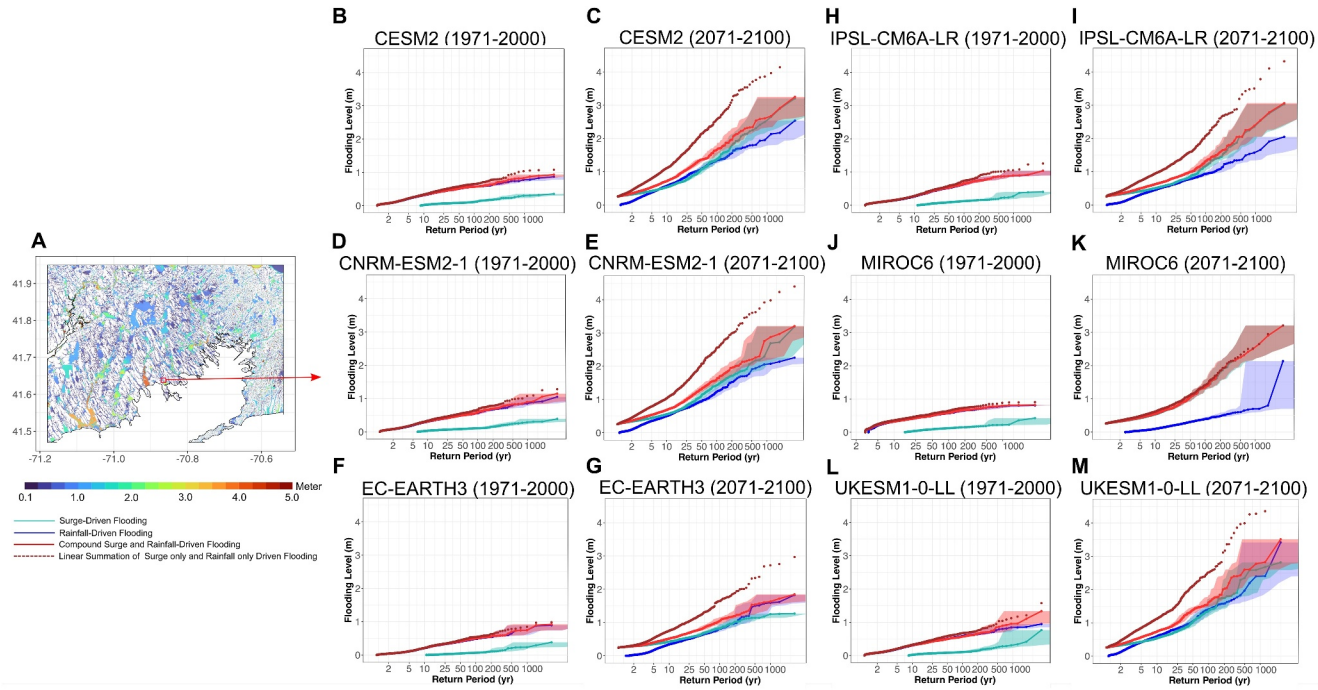

Figure 3. Comparison of compound flooding hazard frequency assessment relative to individual surge and rainfall-driven flooding, and linear addition of individual hazards. (a) Maximum compound flooding level from a randomly selected synthetic TC generated from the EC-EARTH3 model during the late 20th century, along with the location of a coastal area chosen for comparing different types of flooding. (b and c) Flooding levels as a function of the return period from various individual and compound flooding hazard sources for the selected coastal area, using synthetic TCs generated from the CESM2 model for the late 20th and 21st centuries, respectively. (d–m) Similar to (b) and (c) but using synthetic TCs generated from other climate models. The shaded areas in the plots represent sampling uncertainty bounds, calculated based on the 5th and 95th percentiles of a Poisson distribution within each climate model.

comparisons are based on the results obtained from six climate models. This approach clarifies differences in flooding sources across models and accounts for uncertainties among them.

To conduct the analysis, we run our model under four distinct scenarios for each TC event. First, we modeled rainfall-driven flooding using only rainfall as the boundary condition. Second, we simulated surge-driven flooding using storm surge as the driver (SLR is incorporated). Third, to capture compound flooding, both primary drivers—rainfall and surge height—were applied simultaneously as boundary conditions, along with SLR, to account for the complex dynamic interplays between these two flooding types during landfall of each event. Fourth, for comparative purposes, we also calculated a scenario where we simply summed the flood levels from the individual rainfall and surge-driven flooding for each event, deliberately ignoring any dynamic interactions between these two sources of flooding during landfall. To better understand the impact of compound flooding on hazard frequency in the late 20th and 21st centuries, we selected a specific coastal urban area, as shown in Figure 3a. This area was chosen to predominantly consist of non-tidal ground areas, with intertidal zones excluded, facilitating a comparative hazard frequency analysis. We evaluated the hazard, defined by probability of occurrence or return period, associated with single hazards: surge-driven flooding (green), rainfall-driven flooding (blue), and compound flooding, which takes into account the complex hydrodynamic interplay between these hazards at high temporal and spatial resolutions (red). We also included a linear addition of individual flooding as a commonly used approach (in brown). This analysis highlights the uncertainties that arise from assessing individual flooding hazards separately or combining them linearly, without considering the hydrodynamic interplay across time and space inherent to compound flooding. Note that for the late 20th century period, we applied a bias correction method using quantile mapping to the levels of different types of flooding, based on the corresponding levels from NCEP reanalysis data (Gudmundsson et al., 2012).

As depicted in Figure 3, during the late 20th century, a significant proportion of compound flooding originated from rainfall-driven flooding rather than surge-driven flooding, for both high-frequency and low-frequency events in nearly all climate models. This emphasizes the hazard frequency underestimation resulting from relying solely on surge-driven flooding in this region. Conversely, the linear summation of the two individual hazards in each event, conducted in a simplistic manner and without accounting for the complex hydrodynamics of their interaction during landfall, typically results in an overestimation of compound flooding and hazard across the majority of climate models. Therefore, relying solely on simple methods, such as hazard assessments based on either surge-driven or rainfall-driven flooding individually, as demonstrated here, leads to an underestimation of hazard. Similarly, simply adding these two hazards together results in an overestimation of hazard. Neither approach is adequate for accurately quantifying the actual level of compound flooding and the associated hazard frequency, especially in rare events. The appropriate method for assessing compound flooding involves simulating the complex hydrodynamics between surge- and rainfall-driven flooding with high spatial and temporal resolution. This approach provides a comprehensive understanding of the dynamics of compound flooding during landfall, and such detailed simulations should be the basis for any risk assessment of compound flooding in coastal areas.

Moving forward to assess the analysis at the end of the 21st century, a significant increase is observed in both individual and compound flooding hazard frequency, driven by alterations in storm climatology and SLR. Compared to the 20th century, the hazard frequency of both rainfall- and surge-driven flooding increases significantly, with surge-driven flooding (partially exacerbated by SLR) dominating compound flooding in this area, especially for low-frequency events (with return periods above 50 years). For specific upper tail low-frequency events, there is a heightened prominence of surge-driven flooding, contributing to compound flooding, compared to rainfall-driven flooding. Additionally, the hazard frequency of compound flooding intensifies; events that occurred once every 100 years in the late 20th century may occur every 5 years by the end of the 21st century in most climate models. It is also worth noting that simply linearly summing the two single hazards together to assess compound flooding results in a significant overestimation of the future flood hazard frequency. For example, events that occur approximately every 500 years (factoring in the complex hydrodynamic interplay between surge and rainfall-driven flooding) are estimated to happen approximately every 75 years by the end of the century when individual hazards are simply added linearly, signifying a considerable bias and overestimation in hazard frequency assessment.

These results highlight the importance of employing a physics-based model for downscaling TCs in a future warming climate. This stands in contrast to relying solely on historical records, which do not accurately represent the characteristics of storms in a different climate, overlooking the profound impacts of climate change on TC behavior. The results also highlight the importance of considering the explicit complex hydrodynamical interplay between the individual flooding hazards in each event when assessing the hazard frequency; this interplay was neglected in previous studies (Emanuel, 2017; A. J. Garner et al., 2017; Lin et al., 2012, 2016; Marsooli et al., 2019; Reed et al., 2015). This leads to a severe underestimation of hazard frequency in current and future climates, with the discrepancy growing as climatology and SLR change.

3.3. Sea Level Rise and Tropical Cyclone Climatology Impacts

SLR and changes in TC climatology are recognized as the primary drivers behind alterations in the hazard of compound flooding in coastal regions. SLR, largely attributed to global climate change, raises the baseline water level and increases coastal inundation risk. When coupled with anticipated shifts in TC climatology, including variations in cyclone tracks, intensification, frequency, and other relevant attributes, the potential for compound flooding becomes increasingly evident. In this section, we investigate the individual and compounding effects of SLR and changes in storm climatology, analyzing their influence on the hazard of compound flooding during the late 20th century and the late 21st century. The late 20th century serves as a baseline for estimating historical trends, while the late 21st-century projection offers insights into warming scenarios.

Figure 4 shows the compound flooding level from a large set of synthetic tracks in the previously selected coastal area (depicted in Figure 3a), both with and without SLR in the late 20th and 21st centuries, based on the output from six climate models. This analysis aims to better quantify the effect of SLR on changing the hazard frequency of compound flooding and associated uncertainty within and among different climate models. Note that compound flooding levels derived from multiple models at the end of the 20th century are bias-corrected based on

10.1029/2024EF005078

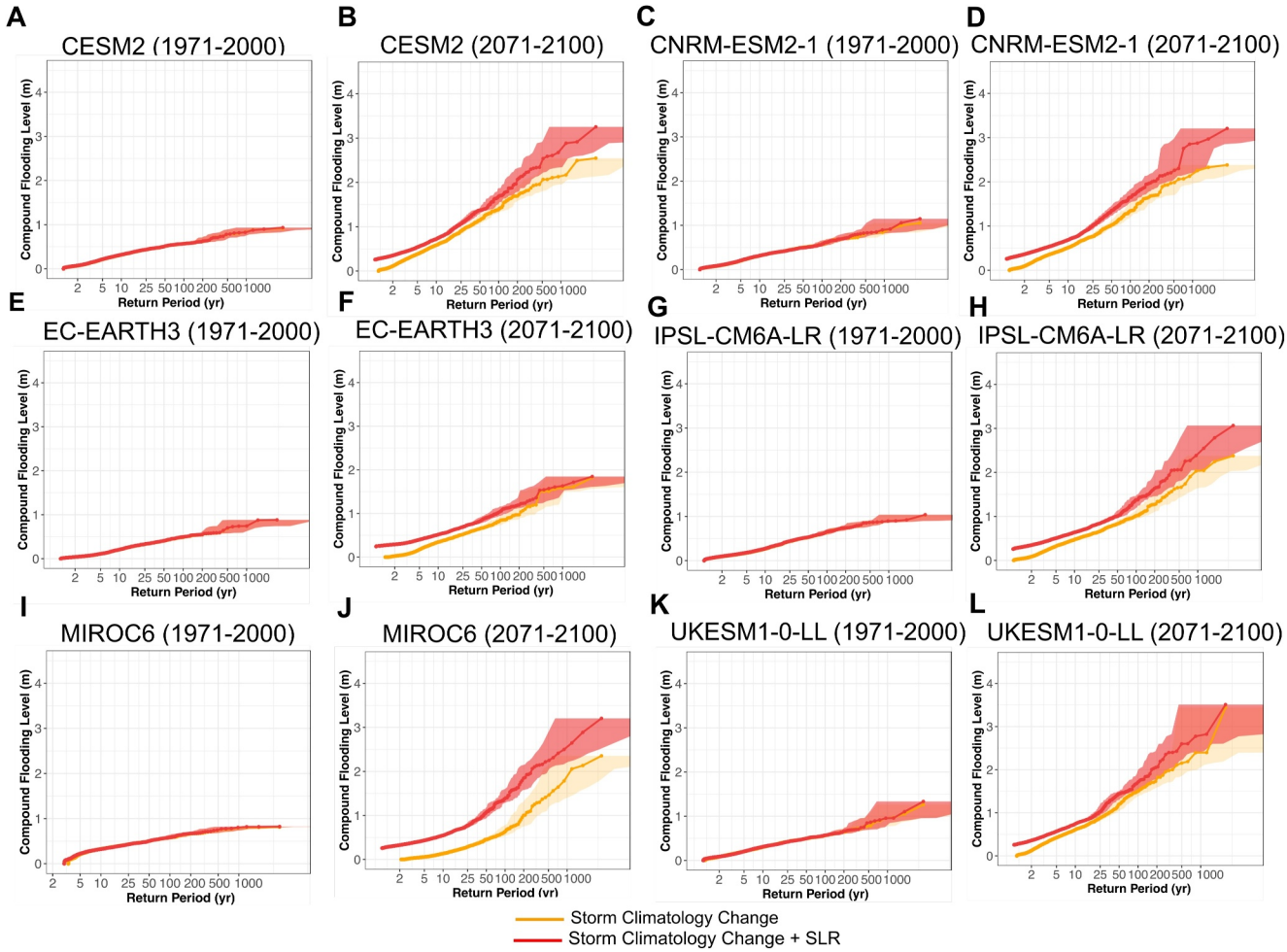

Figure 4. Assessment of the contribution of SLR and changes in TC climatology to the hazard of compound flooding in the late 20th and 21st centuries, focusing on the selected location depicted in Figure 3a. Each line in the graph illustrates the simulated compound flooding levels derived from synthetic TCs downscaled from each of the six climate models. The shaded region represents the confidence interval, indicating sampling uncertainty, and is calculated based on the 5th and 95th percentiles of a Poisson distribution within each climate model.

compound flooding levels from the NCEP reanalysis. In the late 20th century, as depicted in Figure 4, SLR does not exhibit a discernible effect on the hazard of compound flooding caused by TCs. During this baseline period, the hazard of experiencing compound flooding with a 0.5-m depth, for example, is approximately 1% per annum on average, based on the ensemble of the six climate models, both with and without SLR. As we progress toward the end of the century, changes in storm climatology, without considering the SLR effect, are projected to elevate the hazard frequency of compound flooding events. For example, this hazard elevation for the same 0.5-m compound flooding event is manifested with a 10% probability per annum, based on the CNRM-ESM2-1 model (Figure 4d). This projection indicates that changes in TC climatology alone will escalate the frequency of such events tenfold compared to the late 20th century. However, when we consider the added contribution of SLR by the end of the century, the hazard frequency of the same compound flooding event will increase significantly. It is projected to occur approximately with a 20% probability per annum. This signifies that the combined impact of SLR and changes in storm climatology will amplify the hazard twentyfold compared to the late 20th century. Furthermore, SLR alone will elevate the occurrence of such compound flooding events tenfold compared to the late 20th century and increase the annual probability of such an event to 10%. Similar intensification patterns are observed in other climate models. The intensification resulting from the combined impact of SLR and changes in storm climatology significantly amplifies the hazard frequency of low-frequency events in the late 21st century. For instance, events that historically had a return period of 1,000 years in the late 20th century are projected to

occur 40 times more frequently by the end of the century in the majority of the models. In terms of the depth of compound flooding events with a return period of 1,000 years in the selected coastal area, the EC-EARTH3 model estimates it to be approximately 0.75 m (ranging from 0.6 to 0.8 m) in the late 20th century. However, by the end of the century, the depth of floods with the same return period is projected to be around 1.65 m (ranging from 1.5 to 1.8 m) due to the combined effects of SLR and changes in storm climatology.

Another noteworthy observation is that SLR is expected to significantly increase the hazard of low-frequency events in the upper tail compared to other medium or high-frequency events by the end of the century. In a warming climate, all climate models (except EC-EARTH3 and UKESM1-0-LL) show that SLR is projected to intensify the hazard significantly for upper tail events. For example, an extreme event that might occur almost once every 2,000 years (based on the CNRM-ESM2-1 model) by the end of the century would have a depth of compound flooding without the impact of SLR at almost 2.4 m. However, with SLR's impact by that time, the depth is projected to increase to around 3.3 m in such a warming climate. This difference is smaller in medium to high-frequency events.

In addition to the impacts of storm climatology changes and SLR between the late 20th century and the late 21st century, we analyze other TC-related factors, including storm frequency, dynamics (upward motion), moisture, duration, and their contributions to changes in TC total rainfall. For this purpose, we employ the methodology introduced by Emanuel (2024). In this analysis, we define a 96-hr window centered on the time when the cyclone center is nearest to the point of interest (New Bedford, in this case) and calculate the total rainfall. For all storms whose exceedance frequency of total rainfall is less than a specified threshold (here, less than one in 200 years, defined as low-frequency events), we calculate the contributions of each aforementioned TC factor for both the late 20th century and the 21st century. For the late 21st century (future climates), we repeat this analysis under two scenarios: first, by maintaining the overall frequency at the late 20th century climate level, and second, by letting the overall frequency equal its value in the future climate. This process is applied to event sets from multiple climate models.

Figure 5 illustrates the contributions of different TC factors with low-frequency 200-year return periods from the late 20th century to the late 21st century. The results show that the increase in total rainfall is predominantly driven by these intensified cyclones, although there is considerable variation across the models. Another significant contribution to these future rare TCs comes from an increase in moisture, with less uncertainty across models due to their agreement on temperature increase. The contribution from changing TC frequency of these rare events tends to increase, albeit with variations among the climate models. The contributions of duration and vertical motion to total rainfall also increase, but are lesser in magnitude compared to other factors by the end of the century, with considerable uncertainty among the models.

Our methodology enables us to examine how these interacting primary drivers may influence the hazard of compound flooding in a warming climate, providing valuable insights into the adaptive strategies and mitigation measures required for the late 21st century to safeguard coastal communities and infrastructure in an evolving climate. These analyses provide detailed granular information about which primary drivers are of greater concern and how adaptive strategies can be tailored for each specific area based on priorities.

3.4. Tropical Cyclone Compound Flooding Hazard in Today's Climate

Here, we use our methodology to quantitatively assess the impact of anthropogenic warming that has already occurred on the hazard frequency of compound flooding, specifically through TC climatology and SLR in the current climate. To achieve this, we simulate the maximum compound flooding levels from 4,100 synthetic TCs. These TCs are downscaled from NCEP reanalysis data for two distinct climate periods: the late 20th century (1979–1999) and the early 21st century (2000–2020). Figure 6a compares the levels of compound flooding events for different return periods between these two time frames, focusing on a selected location close to the shore, containing buildings and road networks.

Our results suggest no significant changes in the hazard of high-frequency events (less than 50 years) in the current climate compared to the late 20th century. However, they suggest a slight increase in the magnitude of compound flooding, characterized by return periods exceeding 50 years, under today's climate compared to the late 20th century. However, it is important to note that distinguishing distinct trends for these events proves challenging due to sampling uncertainties.

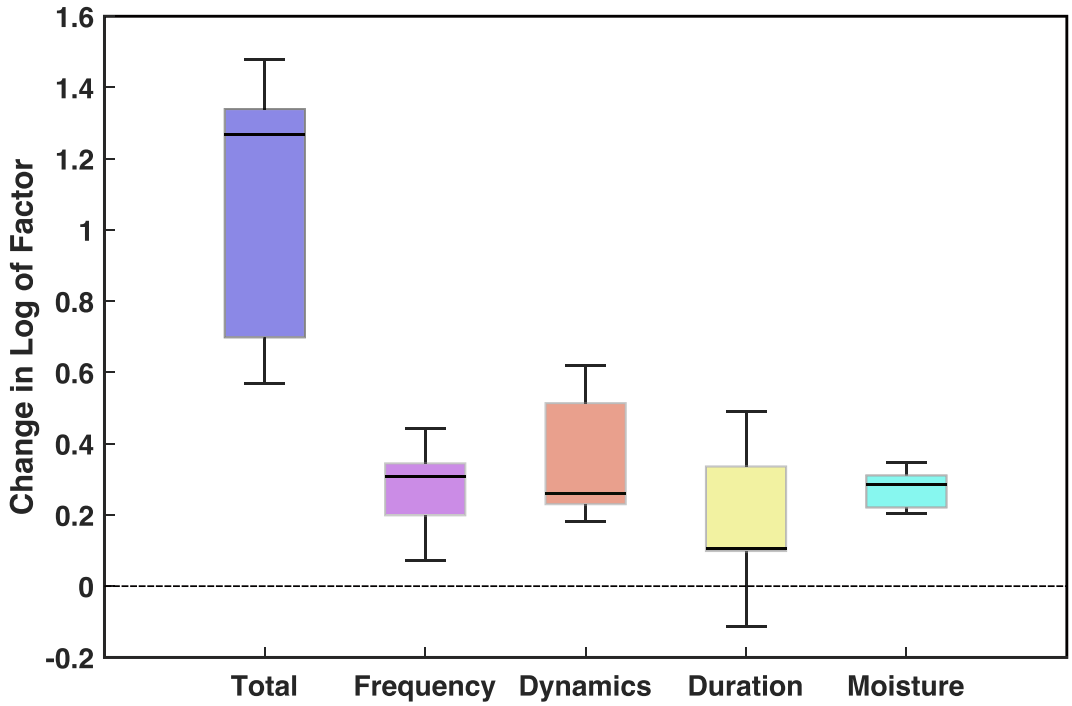

Figure 5. Changes in the logarithmic contributions of various factors to TC total rainfall at a 200-year return period, from the historical (late 20th century) to the future climate (late 21st century). The boxplots extend from the lower to the upper quantiles of the distribution across multiple climate models, with the horizontal line representing the multimodel median.

In Figure 6b, we present the spatially distributed hazard of compound flooding events that occur once every 100 years, or with a 1% likelihood in any given year, across the entire study area. Notably, there is no observed decreasing trend in flooding levels for such events within the region. The results indicate that changes in TC storm climatology, particularly increased rainfall in the current warming climate relative to the late 20th century, have raised flooding levels by up to 0.4 m in low-lying coastal and inland areas, although this increase is not significant given the sampling uncertainty shown in Figure 6a. While SLR is also considered as a contributing factor, it does not have a significant impact on compound flooding levels. Therefore, the majority of changes, especially in inland areas, are primarily attributed to changes in TC climatology.

3.5. Tropical Cyclone Compound Flooding Hazard in a Warming Climate

Here, we conduct a comprehensive analysis of compound flooding hazard frequency associated with TCs, focusing on how this hazard may evolve in a warming climate. Our investigation considered changes in TC climatology and SLR across different time periods. To understand the temporal evolution of compound flooding hazard in our study area, we center our analysis on a specific location near New Bedford City, as indicated in Figure 6a. Our aim is to illuminate the changing dynamics of compound flooding depths in this area, drawing insights from historical data, contemporary observations, and future climate projections.

We conducted a rigorous probabilistic analysis, using advanced mixture modeling techniques to estimate the probability distributions of compound flooding for each time period. Specifically, gamma and Weibull mixture models were applied to simulated compound flooding levels from each climate model, with model selection guided by the Akaike Information Criterion (AIC) (Bozdogan, 1987). To comprehensively assess inherent uncertainty, we applied bootstrap resampling techniques, generating 3,000 samples per iteration for compound flooding level simulations from each climate model across each time period. Subsequently, confidence intervals at the 5% and 95% levels were derived for key parameters associated with the fitted distribution. The frequency of compound flooding in the specified regions, attributed to changes in storm climatology and SLR, is delineated in Figure 7 through aggregated simulations involving six CMIP6 climate

10.1029/2024EF005078

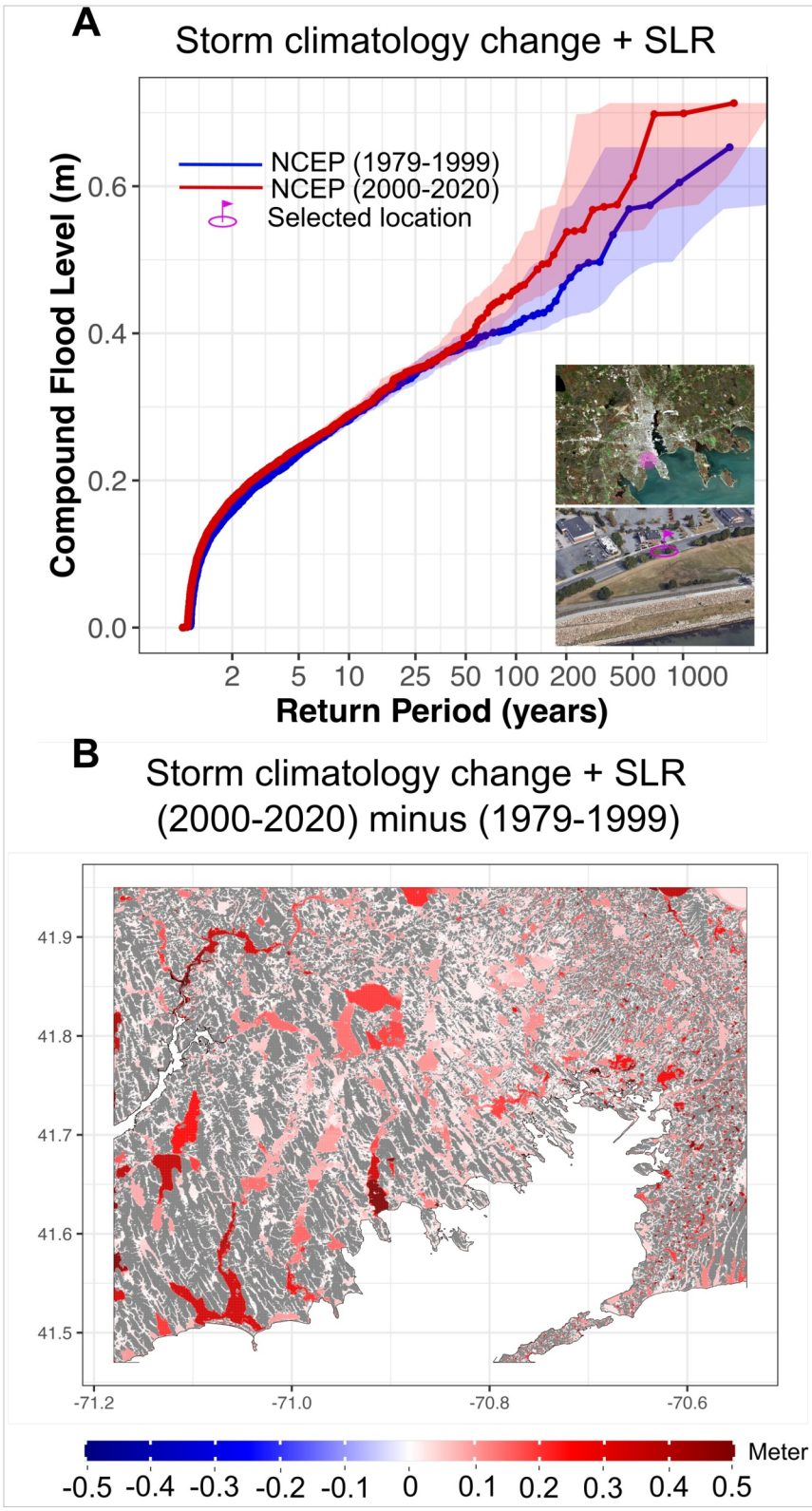

Figure 6.

models. In this figure, the bold line represents the frequency of compound flooding levels within the selected area for different return periods across distinct time periods, including simulations for the late 20th and 21st centuries, as well as reanalysis data from the NCEP data set for the current climate (2000–2020). Furthermore, the colored envelope illustrates the ensemble mean within the 5th to 95th percentile range, calculated based on the outcomes derived from the six climate models. The results (based on the ensemble mean of the climate models) indicate that compound flooding events that previously occurred with a 1% probability in a given year, in the late 20th century in this particular location, have now increased in frequency. In the current climate, these events occur with an annual probability of 1.3% in any given year, and in the future, they are expected to occur with a probability of 3.3% in each year. Changes in storm climatology and SLR are leading to a significant increase in the hazard frequency of compound flooding in the selected area. Furthermore, the depth of compound flooding associated with low-frequency events from TCs will also substantially increase. For instance, for events with an annual probability of 0.2%, the depth of compound flooding in this specific area is projected to rise from approximately 0.5 m in the current climate to 1.25 m by the end of 21st century. Therefore, it is important that the design of infrastructure, housing, and other critical facilities takes into account the heightened hazard of compound flooding from TCs, both in the present and in the face of future, intensifying storms and SLR.

To gain a comprehensive understanding of the spatially distributed hazard of compound flooding in the area, we have calculated the hazard for each grid cell with a 20-m spatial resolution based on extensive synthetic TC simulations. Figure 8 illustrates the results for different types of compound flooding events with return periods of 5, 50, 200, and 500 years. This spatial analysis provides valuable insights into the hazard frequency associated with both high-frequency and low-frequency compound flooding events from TCs. For each time period, including the late 20th century (Figures 8a–8d) and the 21st century (Figures 8e–8h), we assessed the depth of compound flooding for various high and low-frequency events at the grid cell level. To understand the role of changes in storm climatology and SLR in reshaping the hazard landscape of compound flooding in a warming climate in the study area, we have used the late 20th century as a baseline for comparison. The ensemble mean of compound flooding for each return period was analyzed to discern trends and shifts in the occurrence and intensity of compound flooding from TCs. Figures 8i–8l reveal that, for high-frequency events, the level of compound flooding resulting from intensified TCs and SLR will increase by 0.5–1.0 m in coastal areas and by 2.0–2.5 m for low-frequency events in the same regions. In inland areas, the hazard of flooding from intensified rainfall associated with TCs in a warming climate will increase significantly, with flooding levels rising by 1.5–2.5 m for low-frequency intensified TCs in the majority of areas.

The detailed, granular information provided in this section regarding compound flooding in the late 20th century and in a warming climate in the late 21st century is crucial for tailoring effective adaptation strategies in infrastructure design, as well as for the construction of buildings and critical infrastructure such as power plants. This information is also important for formulating policies and structuring insurance to discourage habitation in high-hazard locations. Relying solely on historical hazard frequency assessments, even when extensive information is available, as depicted in Figures 8a–8d, is insufficient. This is because the risk of compound flooding driven by TCs in future warming decades will surpass historical hazard due to changes in storm climatology and SLR (Figures 8e–8h). Our physics-based risk assessment methodology provides a comprehensive understanding of the compound flooding hazard linked to TCs, spanning historical, current, and future scenarios. Through the comparative analysis of return periods across different temporal frames, our findings serve to inform and direct strategies for mitigating and adapting to the complex challenges presented by compound flooding in a continually evolving climate. Therefore, it is desirable to ground design decisions in physics-based hazard assessment outcomes tailored to the future climate to establish resilience in infrastructure, urban development, and community preparedness.

Figure 6. Impact of TC climatology change and SLR on the alteration of compound flooding hazard during today's climate (2000–2020) in comparison to the late 20th century (1979–1999) in a selected coastal location. (a) Representation of the compound flooding levels as a function of return period, comparing today's climate with the late 20th century. The results are derived from the depicted coastal location, excluding intertidal zones. Each line represents compound flooding outcomes produced through the generation of synthetic TCs based on reanalysis NCEP data for the respective time periods. The shaded areas in the figure indicate the sampling uncertainty margins, calculated using the 5th and 95th percentiles of a Poisson distribution. (b) Assessment of the impact of changes in TC climatology and SLR on the spatially varying hazard of 100-year return period compound flooding events in today's climate relative to the late 20th century. In this map, red color denotes an increasing trend, blue color represents a decreasing trend, and gray color signifies areas exhibiting no discernible trend or values close to zero.

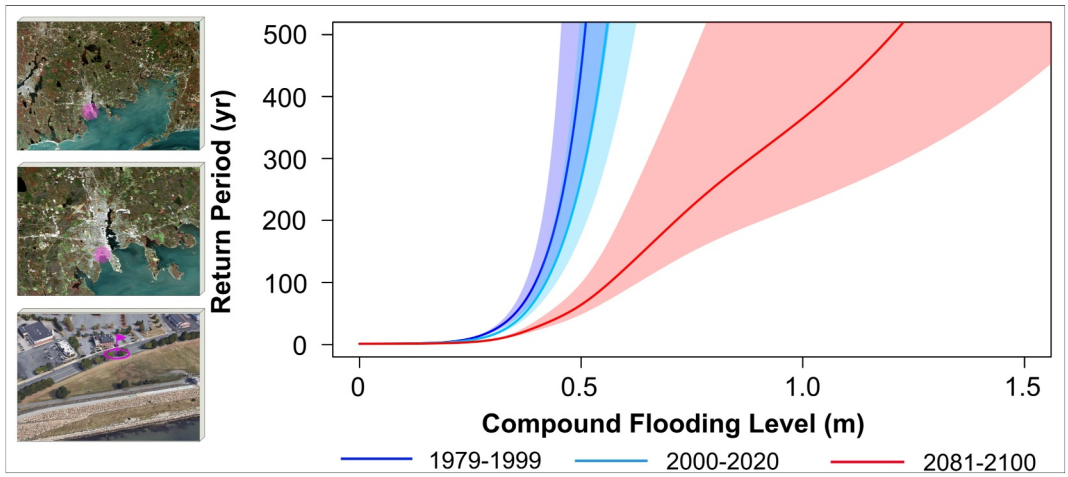

Figure 7. Impact of TC climatology changes and SLR on compound flooding in historical, present, and future climates in the selected coastal area (depicted in the left panels). Each line represents the outcomes derived from synthetic TCs downscaled from multiple climate models and reanalysis data for the three timeframes: historical (dark blue), present (light blue), and future climates (red). The shading in the figure represents confidence intervals (5% and 95%) derived through a bootstrapping approach for the ensemble of climate models. See text for details.

3.6. Assessing Compound Flooding Effect From Extratropical Cyclones

In this section, we analyze compound flooding from ETCs, emphasizing the importance of dynamic interactions compared to methods that assess singular hazards or use linear additive approaches, which may underestimate or overestimate hazard frequency. To better understand the impact and importance of the complex dynamic of compound flooding in hazard frequency assessment in both the current and the later 21st century climates from ETC events, we selected a specific coastal area, which is also an urban area, as depicted in Figure 9a. This area was chosen to predominantly consist of non-tidal ground areas, with intertidal zones excluded, facilitating a comparative hazard frequency analysis.

We emphasize that our ETC hazard frequency analysis is very limited compared to our analysis of TC hazard, owing to the great computational expense of downscaling ETCs, as discussed in Section 2.2. We are here limited to using a single climate model run over limited spans of time and so considering only high frequency events, constrained as we are by the use of a previously generated ETC direct downscaling. We include this more limited hazard frequency analysis primarily to demonstrate that we can apply and learn from the same approach to compound flooding that we applied to TCs and in the hopes that we someday will do a more thorough analysis of ETC compound flood hazard analysis once suitable high-resolution data sets become available.

Figure 9b illustrates that in the current climate, a substantial portion of the contributions to compound flooding in high-frequency events stems from rainfall-driven, rather than surge-driven, flooding. This highlights the potential for underestimating hazards when solely considering surge-driven flooding in this region. Note that the lower values for surge-driven flooding are associated with the selected area that intentionally extends inland, specifically to exclude any intertidal zones. Conversely, the simplistic linear addition of these two individual hazards—without considering the complex hydrodynamics of their interaction during landfall—leads to an overestimation of hazard for high-frequency ETC events (with a return period of 20 years or less). Looking ahead to the end of the 21st century, there is a notable increase in both individual and compound flooding hazards, driven by changes in storm climatology and SLR. While hazards from both rainfall-driven and surge-driven flooding show significant increases compared to the current climate, surge-driven flooding becomes more dominant and contributes more substantially to compound flooding than rainfall-driven flooding in this area for high-frequency ETC events. Additionally, it is important to note that the mere linear combination of these two single hazards to assess compound flooding leads to biases and overestimates of the hazard in the future climate scenario.

The results emphasize the need to account for the complex hydrodynamic interactions between individual flooding hazards for each event when evaluating the hazard frequency. Neglecting these dynamics, as seen in the

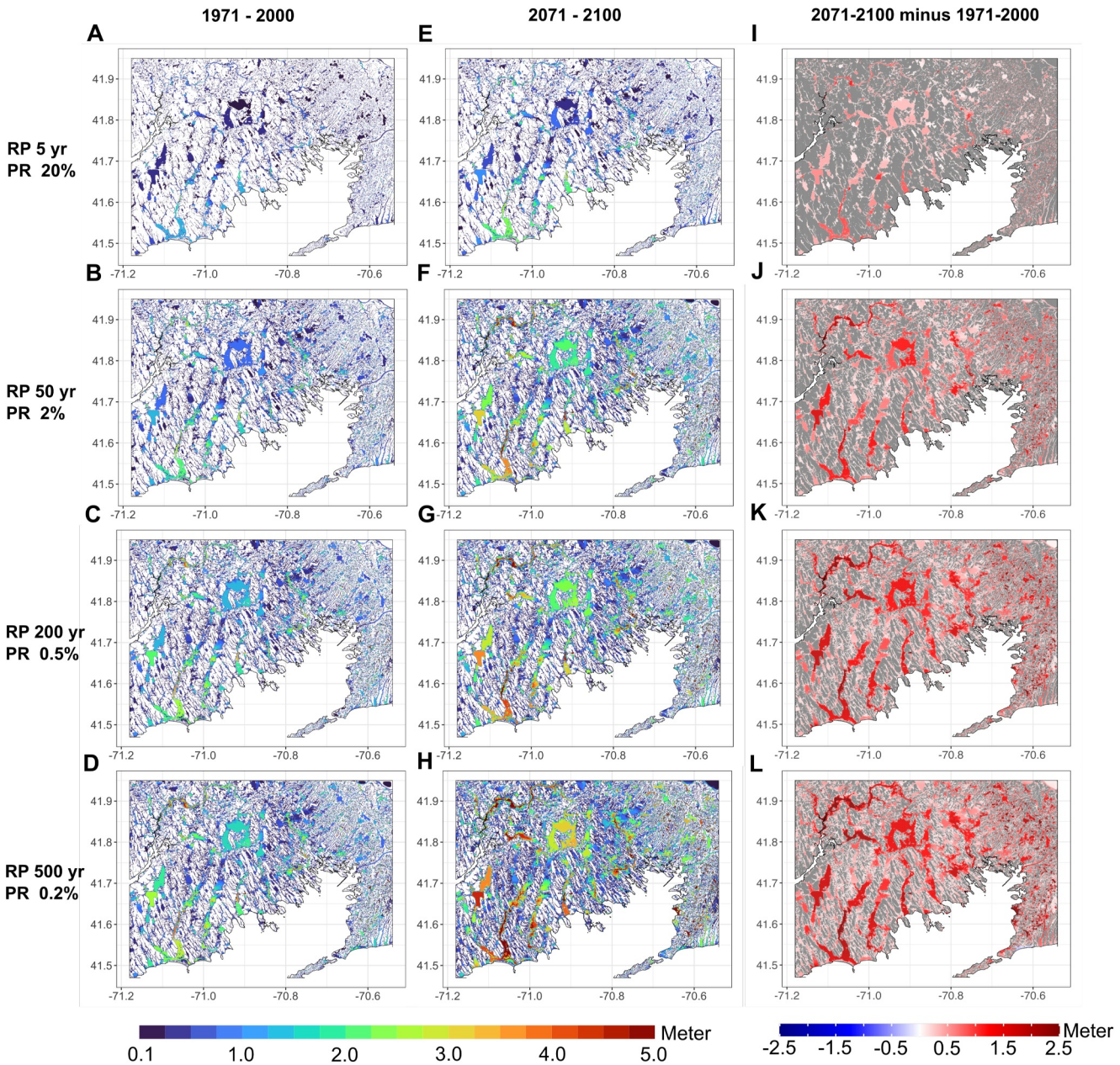

Figure 8. Spatially distributed granular hazard of compound flooding from TCs in past and future climates. (a–d) Present the results of compound flooding for various return periods in the late 20th century. (e–h) Depict the same analysis for the late 21st century. (i–l) Illustrate the differences in compound flooding levels between the late 21st century and late 20th century for different return periods. Here, red indicates an increasing trend, blue indicates a decreasing trend, and gray signifies no clear trend or values close to zero. Note that these results are based on the ensemble mean of the six CMIP6 climate models.

previous studies (Lin et al., 2019; Roberts et al., 2017) can result in an underestimation of the actual hazard in both current and future climates. This discrepancy is likely to become more pronounced with changes in ETC climatology and SLR as depicted in Figure 9c.

3.7. Sea Level Rise and Extratropical Cyclone Climatology Impacts

Here, we assess the impacts of individual and combined primary drivers—SLR and changes in ETC climatology—on the hazard of compound flooding from high-frequency ETC events in both current and late-century climates. Figure 10 illustrates the levels of compound flooding in a previously selected coastal area (depicted in Figure 9a),

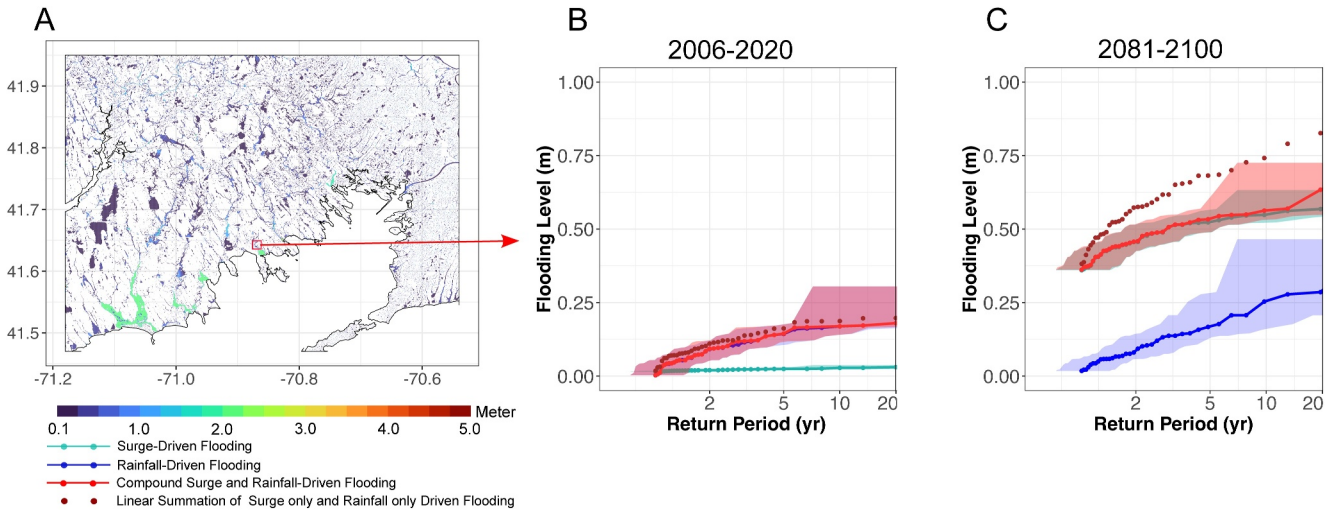

Figure 9. Comparison of ETC compound flooding hazard frequency assessment relative to individual surge and rainfall-driven flooding, and linear addition of individual hazards. (a) Maximum compound flooding level from a randomly selected dynamically downscaled ETC during current climate, along with the location of a coastal area chosen for comparing different types of flooding. (b) Flooding levels as a function of the return period from various individual and compound flooding hazard sources for the selected coastal area, in the current climate (2006–2020). (c) Similar to (b) but for the late 21st century (2081–2100). The shaded areas in the plots represent sampling uncertainty bounds, calculated based on the 5th and 95th percentiles of a Poisson distribution.

highlighting the effects due to changes in climatology (represented in orange) and the combined effects of climatology changes and SLR (represented in red) under two different climates.

In the current climate, SLR has a negligible impact on the hazard of compound flooding from ETCs (Figure 10a). However, by the end of the century, while changes in climatology may slightly increase the hazard of compound flooding for events with a return period of 20 years or less, these changes are not significant when compared to the current climate (Figure 10b). Conversely, the combined impact of ETC climatology changes and SLR is projected

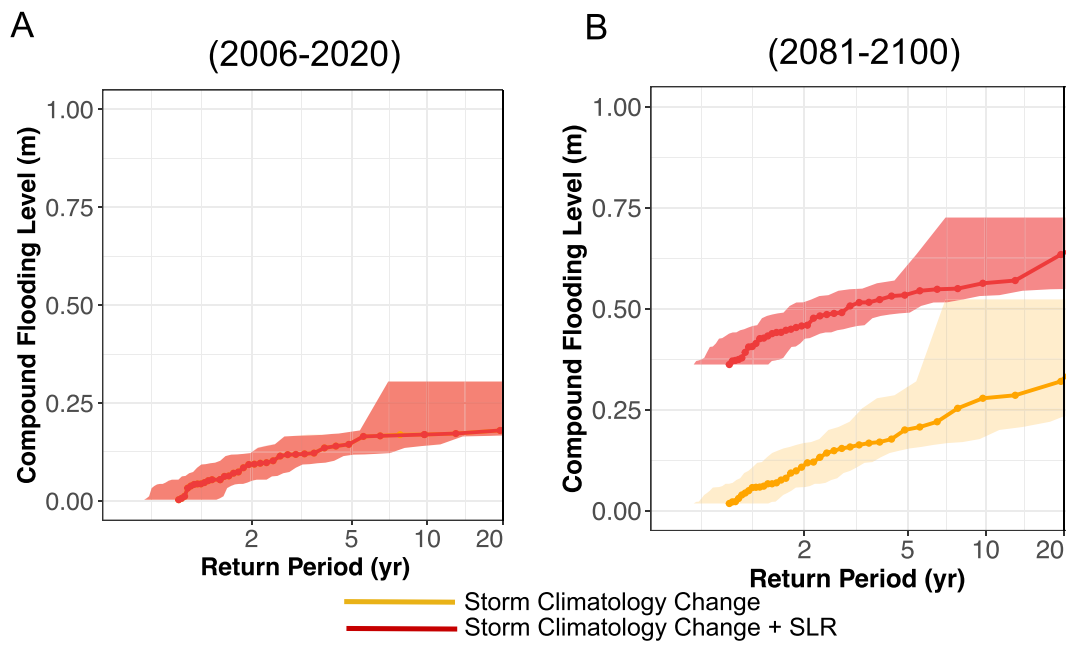

Figure 10. Assessing the contributions of SLR and ETC climatology changes to the hazard of compound flooding in the current climate and the late 21st century, focusing on the location shown in Figure 9a. Each line in the graph represents simulated compound flooding levels from dynamically downscaled ETCs. The shaded region, representing the confidence interval that indicates sampling uncertainty, is calculated based on the 5th and 95th percentiles of a Poisson distribution.

10.1029/2024EF005078

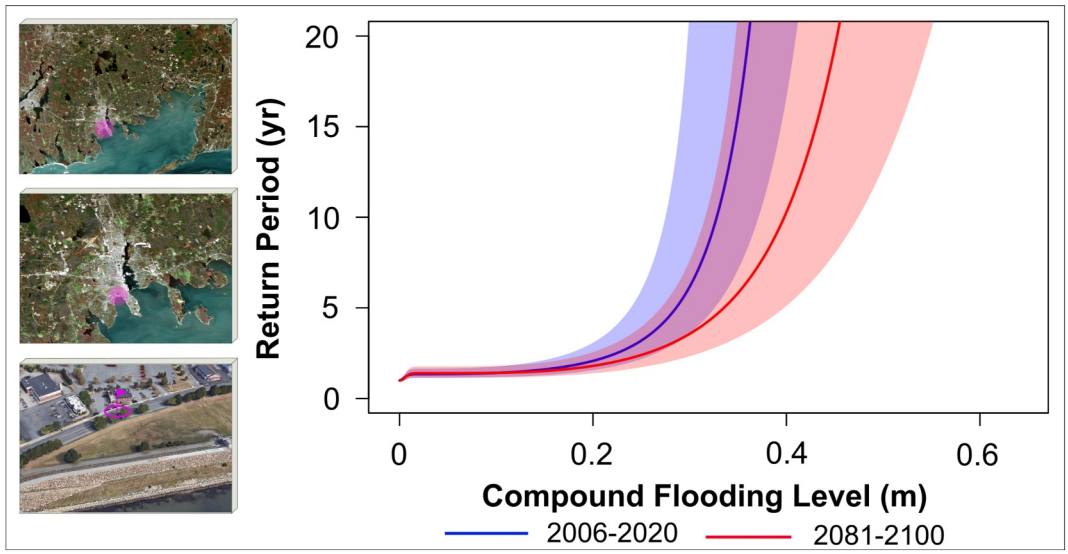

Figure 11. Impact of ETC climatology changes and SLR on the hazard of compound flooding in the current and future climates in the selected coastal area (depicted in the left panels). Each line represents the outcomes derived from dynamically downscaled ETC events for two timeframes: the current climate (2006–2020, shown in blue) and future climates (2081–2100, shown in red). The shading in the figure represents confidence intervals (5% and 95%) derived through a bootstrapping approach.

to significantly alter the hazard of compound flooding compared to the current climate, with the majority of changes attributable to SLR rather than to alterations in storm climatology. For instance, for ETC compound flooding events occurring once every 20 years, the level of compound flooding is approximately 0.35 m when considering only climatology changes; however, this level rises to about 0.63 m when SLR is also factored in. Therefore, compared to the current climate, the results suggest that SLR is likely to be the dominant factor increasing the hazard of compound flooding, particularly for high-frequency ETC events in coastal areas in the coming decades. Once again, the limitations of the downscaled data set we used prevent us from a robust assessment of low frequency ETC events.

3.8. Extratropical Cyclone Compound Flooding Hazard in Current and Future Climates

In Figure 11, we illustrate the contributions of ETC climatology changes and SLR to variations in compound flooding hazards in the depicted area for both current and future warming climates. Our analysis is limited to high-frequency events, defined by return periods of 20 years or less, due to constraints associated with our downscaled data set. The combined impact of ETC climatology changes and SLR is expected to nearly triple the likelihood of compound flooding by the end of the century in the selected coastal area. Specifically, compound flooding events with high-frequency occurrences, with a 5% annual probability, are expected to occur with a 14% annual likelihood by the end of the century. These pronounced changes are primarily observed in the coastal areas. Similar high-frequency events stemming from TCs, as depicted in Figure 7, are projected to occur with an 11% annual likelihood by the end of the century. While the scenarios differ (RCP8.5 vs. SSP3-7.0), the probability of such compound flooding events arising from ETCs is slightly, yet not significantly, higher under RCP8.5 (considered a high-end warming scenario). While it appears that the hazard of high-frequency compound flooding will increase comparably for both TCs and ETCs, a consistent warming scenario is essential for a comprehensive comparison not only of high-frequency but also low-frequency compound flooding events from TCs and ETCs in the future climate.

To gain deeper insights into the effects of ETC climatology change and SLR, we also quantify the spatially varying hazard of compound flooding events in the current and future warming climate. Figures 12a–12d depict the results for the current climate, while Figures 12e–12h display the projections for the end of the century. In Figures 12i–12l, we highlight differences in flooding levels across the area for the specified return periods. Evidently, coastal areas exhibit a pronounced intensification of compound flooding, attributed primarily to SLR within these regions. The magnitude of this intensification in compound flooding levels increases from events

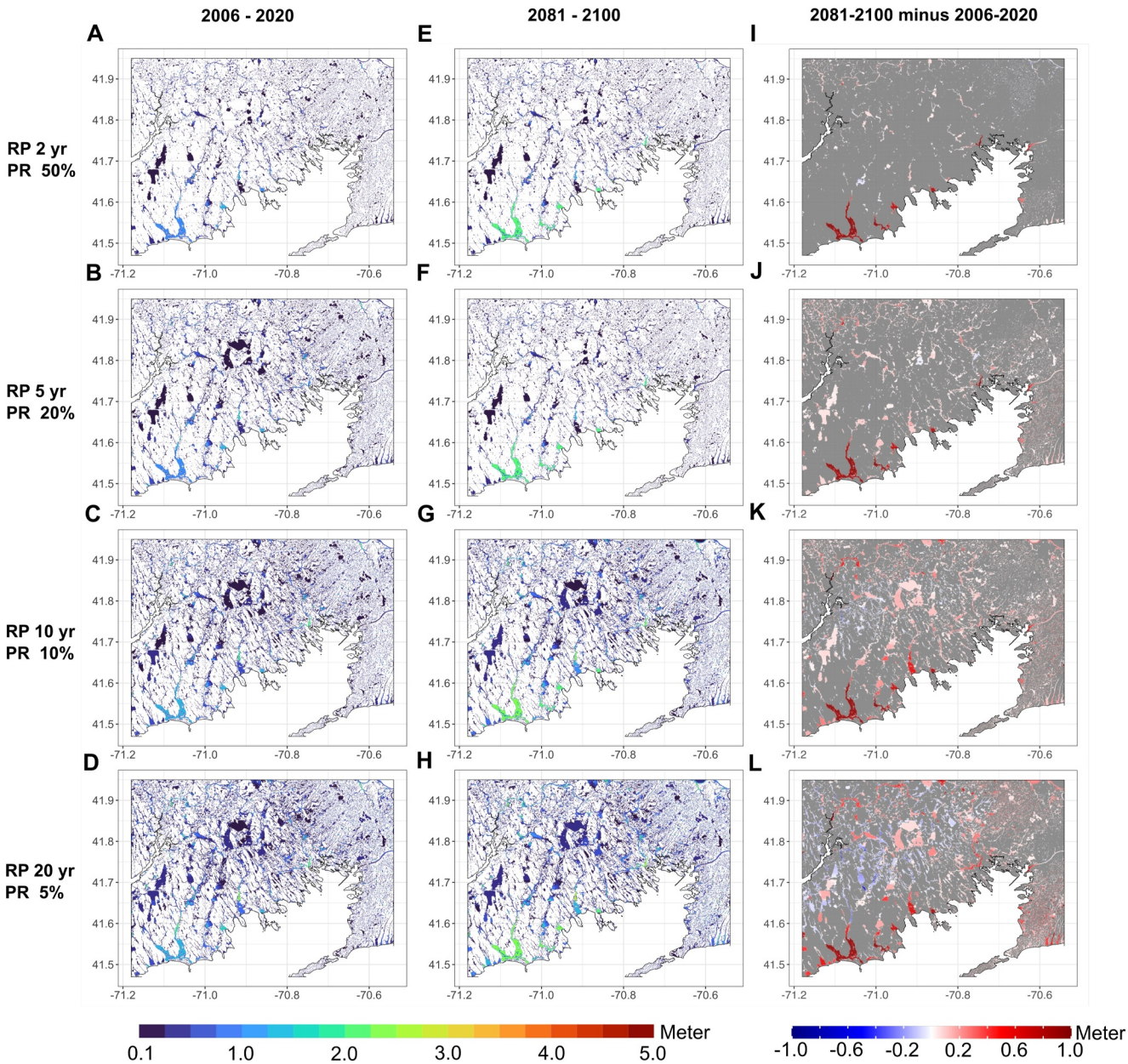

Figure 12. Spatially distributed granular hazard of compound flooding from ETCs in the current and future climates. (a–d) Present the results of compound flooding for various return periods in the current climate. (e–h) Depict the same analysis for the late 21st century. (i–l) Illustrate the differences in compound flooding levels between the late 21st century and the current climate for various return periods. Note that red indicates an increasing trend, blue indicates a decreasing trend, and gray signifies no clear trend or values close to zero.

with return periods of 2 years to those with return periods of 20 years. However, unlike TC-driven compound flooding, the levels of flooding resulting from ETC events in inland areas display a distinct pattern for high-frequency ETC events. Our findings indicate no discernible trend in terms of flooding levels in inland areas at the end of the 21st century, relative to the current climate. In fact, some areas even exhibit a decreasing trend, with only some low-lying regions displaying an increasing trend, which is not statistically significant when compared to the current climate. Therefore, our results suggest that rainfall-driven flooding from high-frequency ETC events will not intensify in inland areas from future ETC events relative to the ones in the current climate. The bulk of the intensification is expected to occur along coastal areas, driven primarily by SLR during high-frequency ETC events. These findings align with prior studies (Booth et al., 2021; Lin et al., 2019), which indicate that the effects of climate change on ETC storms are relatively minor compared to the significant impact

of SLR on storm surge intensification in northeastern U.S. coastal areas. To improve understanding and enable more comprehensive comparisons, it is imperative to include more dynamically downscaled ETC events over longer time periods, particularly focusing on low-frequency events. This would allow us to comprehensively assess the hazard of compound flooding associated with these low-frequency ETC events, similar to the approach taken in our analysis of TC-driven compound flooding events.

4. Conclusion

In this study, we employed a physics-based hazard frequency assessment methodology designed to quantify the frequency of compound flooding stemming from tropical and extratropical cyclones in coastal regions. We highlight the advantages of a physics-based approach, which overcomes the limitations of historically based assessments due to short records and their decreasing relevance in a changing climate. Such methods are essential for understanding the evolving landscape of compound flooding hazard in coastal areas within the current and future climates. Our methodology offers a comprehensive means of assessing past, present, and future hazards under the influence of changing storm drivers and SLR, which amplifies coastal flooding.

To achieve our objectives, we employed a two-pronged approach. First, we downscaled from reanalyses and climate models comprehensive data sets of synthetic TCs using a statistical-deterministic method. Additionally, we assessed ETC compound flood hazard using WRF-based downscaling of a single climate model, to demonstrate that our compound flood model can be applied to ETCs as well as to TCs. These simulations were informed by key climate statistics and reanalysis data, addressing the challenges associated with the scarcity of relevant data sets across time periods. Furthermore, this approach allowed us to account for the influence of climate change on the primary drivers of compound flooding. In order to quantify the hazard of compound flooding, our methodology explicitly considers the intricate hydrodynamics of this phenomenon. It takes into account the simultaneous interplay of surge-driven and rainfall-driven flooding across time and space during the landfall of each storm. This unique approach enables us to assess the contributions and magnitudes of primary drivers, such as rainfall intensity, wind speed, and SLR, in amplifying compound flooding and backwater effects across both time and space at high resolution. It also facilitates the assessment of the contribution of each individual flooding type to the overall compound flooding hazard frequency assessment. Our results highlight the underestimated risks of individual flooding hazards from TCs and ETCs, particularly in a warming climate. This demonstrates the significance of using numerical simulations that incorporate the complex hydrodynamics of explicit compound flooding caused by TCs and ETCs. This approach emphasizes the importance of moving away from reliance solely on statistical joint distribution of the drivers of compound flooding or conventional statistical or physical methods that focus exclusively on individual drivers or hazards (A. J. Garner et al., 2017; Gori et al., 2022; Lin et al., 2016, 2019; Moftakhari et al., 2017; Reed et al., 2015).

Our methodology is essential for understanding the contribution of storm climatology changes and SLR to the evolution of compound flooding hazard over time. We find that TC-driven compound flooding hazard is considerably higher than that of ETC-driven events, for high-frequency events in the Buzzards Bay area. The very limited ETC data set available to us precludes such a comparison for low frequency events. Our results demonstrate an increased hazard of TC-driven compound flooding in the present climate compared to the late 20th century, with significant intensification anticipated in warming climates. SLR emerges as a substantial contributor to this heightened hazard. These results align with the findings of Gori et al. (2022) and Little et al. (2015), who demonstrated that SLR is the primary driver of increased hazard of flooding from TCs in the northeastern U.S. for future scenarios. In the case of high-frequency ETC-driven compound flooding, we anticipate an amplified hazard in coastal areas by the end of the century, primarily due to SLR. Although storm surge is only one component of compound flooding, Lin et al. (2019) demonstrated a slight increase in the hazard of storm surge from high-frequency ETCs in the study area over the coming decades, based on projections using the CMIP5 RCP8.5 scenario. However, their analysis did not incorporate the significant impact of SLR, which our study shows is likely to further exacerbate this hazard. Nevertheless, the hazard in inland areas seems to remain relatively stable, with specific areas even experiencing a reduced hazard of rainfall-driven flooding.

Our methodology for quantifying the hazard of TC compound flooding is particularly effective, even for very low-frequency events, due to our ability to generate an almost unlimited number of synthetic cyclones. In contrast, our capacity to assess the hazard associated with ETCs is significantly constrained by the limited number

of events that can be simulated with complex, three-dimensional models such as WRF. This constraint is primarily due to the extensive computational resources required for such detailed simulations, which are necessary to accurately compare the hazards of compound flooding from TCs and ETCs, especially for rare events under the same warming scenarios. Future research should focus on developing more efficient techniques for downscaling ETCs to enable such comparison. One promising approach involves running ensembles of high-resolution CMIP6 global climate models for both current and projected future climates. This strategy would allow researchers to derive ETC climatology directly from model outputs, providing a more comprehensive understanding of ETC behavior, especially for rare events under various climate scenarios. This approach facilitates a direct, like-for-like comparison of the hazard and risk of compound flooding from TCs and ETCs across various return periods. However, this method would require considerable computational power and data analysis capabilities, highlighting the need for significant investment in high-performance computing resources. This will be a critical next step in advancing this study. Though our study did not address the interaction of astronomical tides with storm surge and SLR, we acknowledge their importance and recommend their inclusion in future assessments of surge and compound flood hazards. Our methodology can be extended beyond the Buzzards Bay area and New York City (Sarhadi et al., 2024) and can be applied as a scalable framework for vulnerable coastal regions worldwide that face the imminent threat of compound flooding from TCs and ETCs, even in the absence of historical records, regardless of their latitude. However, it is essential to tailor the methodology to incorporate region-specific factors, such as bathymetry, soil characteristics, coastal morphology, storm surge dynamics, and tidal influences. Customization helps ensure the accurate assessment and quantification of the compound flooding hazard by tailoring the approach to regional characteristics and conditions.

Our methodology equips decision-makers with scientific insights to strengthen coastal preparedness and resilience. It enables authorities to estimate the likelihood of destructive storms in both current and future decades and quantify potential damages. Regional assessments empower authorities to customize adaptation strategies, allocate resources effectively, and safeguard critical infrastructure and coastal communities. Our study can serve as a cornerstone for proactive hazard frequency assessment, especially given the projected population increase within flood-prone coastal zones and megacities by 2050 (Aerts et al., 2014; Kulp & Strauss, 2019; Neumann et al., 2015). Notably, despite the significant assets in coastal flood-prone areas, investments in protective measures often fall short. Our methodology provides a comprehensive guide to ensure that adaptation efforts are precisely tailored to address the unique challenges posed by compound flooding in coastal cities. In addition to localized adaptation measures, the need to reduce greenhouse gas emissions takes center stage in mitigating the increased risk and reducing associated damages within a warming climate.

In summary, our research advances the ability to assess the multifaceted hazards of compound flooding while providing decision-makers with an analytical framework to strengthen the resilience of vulnerable coastal regions against climate change. Consequently, our study can serve as an essential foundation for the development and implementation of comprehensive strategies encompassing damage mitigation, strategic design, anticipatory planning, predictive forecasting, adaptive measures, and proactive mitigation interventions, all specifically tailored to address the complexities of coastal flooding caused by cyclonic storms.

Data Availability Statement

All data and software used in this study are openly available and can be accessed through the following sources:

All publicly accessible data sets used in this study are referenced and can be accessed as follows:

- Historical SLR data: Available from NOAA (2023b).
- CMIP6 SLR projections: Provided by G. Garner et al. (2022) under the SSP3-7.0 scenario.
- Bathymetry and coastal features: Available from NCEI (2023).
- LiDAR-based Digital Elevation Model: With a resolution of $\sim$20 *m*, obtained from NOAA (2023a).
- Land-use map: Accessible from Wickham et al. (2023).
- Soil available water storage data: Provided by USDA (2023).
- NEXRAD radar-based rainfall intensity data: Accessible from NOAA (2024).
- Flood level data: From USGS gauge station 01105933 for the 27–28 December 2012, ETC event from USGS (2024).
- IBTrACS data: Version 4, accessible from Knapp et al. (2018).

All ETC events, produced by Komurcu et al. (2018), and the codes used in this study are available from Zenodo (Sarhadi, 2024). TC track data are proprietary and licensed under WindRiskTech L.L.C. Access to these data for scientific research purposes is available upon request to the co-author, Kerry Emanuel (emanuel@mit.edu), and is subject to the terms of a licensing agreement.

- LISFLOOD-FP model: The LISFLOOD-FP v8.2 hydrodynamic model utilized in this study is openly accessible on Zenodo at https://doi.org/10.5281/zenodo.13121102 (LISFLOOD developers, 2020). The software is distributed under the General Public License v2.0, and the repository provides documentation, including user guides and scripts.
- GeoClaw model: The GeoClaw v5.8.2 model, utilized for simulating storm surges in this study, is part of the Clawpack suite of numerical modeling tools. GeoClaw is available through the Clawpack repository at https://zenodo.org/records/5781749 (Clawpack Development Team, 2021). The software is distributed under the BSD 2-Clause "Simplified" License and includes documentation, detailed installation instructions, and reproducibility guidelines.

Acknowledgments
The authors express their gratitude to Muge Komurcu, Matthew Huber, and Stanley Glidden for providing WRF dynamical downscaling data for ETC events. We also acknowledge the World Climate Research Programme, which, through its Working Group on Coupled Modeling, coordinated and promoted CMIP. We thank the leading research centers including the National Center for Atmospheric Research, the Centre National de Recherches Météorologiques, the EC-EARTH consortium, the Institut Pierre-Simon Laplace, the Atmosphere and Ocean Research Institute in collaboration with the National Institute for Environmental Studies and the Japan Agency for Marine-Earth Science and Technology, and the Met Office Hadley Centre. These institutions have contributed significantly by producing and making available their climate model outputs. Financial support for this work was provided by Homesite Insurance.

References

Aerts, J. C., Botzen, W. W., Emanuel, K., Lin, N., De Moel, H., & Michel-Kerjan, E. O. (2014). Evaluating flood resilience strategies for coastal megacities. *Science*, *344*(6183), 473–475. https://doi.org/10.1126/science.1248222

Bakkensen, L. A., & Mendelsohn, R. O. (2019). Global tropical cyclone damages and fatalities under climate change: An updated assessment. *Hurricane risk*, 179–197.

Bates, P. D., Horritt, M. S., & Fewtrell, T. J. (2010). A simple inertial formulation of the shallow water equations for efficient two-dimensional flood inundation modelling. *Journal of Hydrology*, *387*(1–2), 33–45. https://doi.org/10.1016/j.jhydrol.2010.03.027

Bates, P. D., Quinn, N., Sampson, C., Smith, A., Wing, O., Sosa, J., et al. (2021). Combined modeling of us fluvial, pluvial, and coastal flood hazard under current and future climates. *Water Resources Research*, *57*(2), e2020WR028673. https://doi.org/10.1029/2020wr028673

Berger, M. J., George, D. L., LeVeque, R. J., & Mandli, K. T. (2011). The geoclaw software for depth-averaged flows with adaptive refinement. *Advances in Water Resources*, *34*(9), 1195–1206. https://doi.org/10.1016/j.advwatres.2011.02.016

Booth, J. F., Narinesingh, V., Towey, K. L., & Jeyaratnam, J. (2021). Storm surge, blocking, and cyclones: A compound hazards analysis for the northeast United States. *Journal of Applied Meteorology and Climatology*, *60*(11), 1531–1544. https://doi.org/10.1175/jamc-d-21-0062.1

Bozdogan, H. (1987). Model selection and Akaike's information criterion (AIC): The general theory and its analytical extensions. *Psychometrika*, *52*(3), 345–370. https://doi.org/10.1007/bf02294361

Clawpack Development Team. (2021). Clawpack software (version 5.8.2) [Software]. *GeoClaw*. https://doi.org/10.5281/zenodo.5781749

Colle, B. A., Booth, J. F., & Chang, E. K. (2015). A review of historical and future changes of extratropical cyclones and associated impacts along the US East Coast. *Current Climate Change Reports*, *1*(3), 125–143. https://doi.org/10.1007/s40641-015-0013-7

Colle, B. A., Buonaiuto, F., Bowman, M. J., Wilson, R. E., Flood, R., Hunter, R., et al. (2008). New York City's vulnerability to coastal flooding: Storm surge modeling of past cyclones. *Bulletin of the American Meteorological Society*, *89*(6), 829–842. https://doi.org/10.1175/2007bams2401.1

Dee, D. P., Uppala, S. M., Simmons, A. J., Berrisford, P., Poli, P., Kobayashi, S., et al. (2011). The ERA-Interim reanalysis: Configuration and performance of the data assimilation system. *Quarterly Journal of the Royal Meteorological Society*, *137*(656), 553–597. https://doi.org/10.1002/qj.828

Dewitz, J. (2021). *US geological survey (2021). National land cover database (NLCD) 2019 products*. US Geological Survey Data Release.

Emanuel, K. (2017). Assessing the present and future probability of hurricane Harvey's rainfall. *Proceedings of the National Academy of Sciences of the United States of America*, *114*(48), 12681–12684. https://doi.org/10.1073/pnas.1716222114

Emanuel, K. (2024). Cyclone jasper's rains in the context of climate change. *Proceedings of the National Academy of Sciences of the United States of America*, *121*(15), e2400292121. https://doi.org/10.1073/pnas.2400292121

Emanuel, K., DesAutels, C., Holloway, C., & Korty, R. (2004). Environmental control of tropical cyclone intensity. *Journal of the Atmospheric Sciences*, *61*(7), 843–858. https://doi.org/10.1175/1520-0469(2004)061<0843:ecotci>2.0.co;2

Emanuel, K., Ravela, S., Vivant, E., & Risi, C. (2006). A statistical deterministic approach to hurricane risk assessment. *Bulletin of the American Meteorological Society*, *87*(3), 299–314. https://doi.org/10.1175/BAMS-87-3-299

Emanuel, K., Sundararajan, R., & Williams, J. (2008). Hurricanes and global warming: Results from downscaling IPCC AR4 simulations. *Bulletin of the American Meteorological Society*, *89*(3), 347–368. https://doi.org/10.1175/bams-89-3-347

Feldmann, M., Emanuel, K., Zhu, L., & Lohmann, U. (2019). Estimation of Atlantic tropical cyclone rainfall frequency in the United States. *Journal of Applied Meteorology and Climatology*, *58*(8), 1853–1866. https://doi.org/10.1175/jamc-d-19-0011.1

Fox-Kemper, B., Hewitt, H., Xiao, C., Aalgeirsdóttir, G., Drijfhout, S., Edwards, T., et al. (2021). Ocean, cryosphere and sea level change.

Garner, A. J., Mann, M. E., Emanuel, K. A., Kopp, R. E., Lin, N., Alley, R. B., et al. (2017). Impact of climate change on New York City's coastal flood hazard: Increasing flood heights from the preindustrial to 2300 CE. *Proceedings of the National Academy of Sciences of the United States of America*, *114*(45), 11861–11866. https://doi.org/10.1073/pnas.1703568114

Garner, G., Hermans, T. H., Kopp, R., Slangen, A., Edwards, T., Levermann, A., et al. (2022). IPCC AR6 WGI sea level projections [Dataset]. *World Data Center for Climate (WDCC) at DKRZ*. https://doi.org/10.5281/zenodo.6382554

Gori, A., & Lin, N. (2022). Projecting compound flood hazard under climate change with physical models and joint probability methods. *Earth's Future*, *10*(12), e2022EF003097. https://doi.org/10.1029/2022ef003097

Gori, A., Lin, N., & Smith, J. (2020). Assessing compound flooding from landfalling tropical cyclones on the North Carolina coast. *Water Resources Research*, *56*(4), e2019WR026788. https://doi.org/10.1029/2019wr026788

Gori, A., Lin, N., Xi, D., & Emanuel, K. (2022). Tropical cyclone climatology change greatly exacerbates us extreme rainfall–surge hazard. *Nature Climate Change*, *12*(2), 171–178. https://doi.org/10.1038/s41558-021-01272-7

Gudmundsson, L., Bremnes, J. B., Haugen, J. E., & Engen-Skaugen, T. (2012). Downscaling RCM precipitation to the station scale using statistical transformations–a comparison of methods. *Hydrology and Earth System Sciences*, *16*(9), 3383–3390. https://doi.org/10.5194/hess-16-3383-2012

Kalyanapu, A. J., Burian, S. J., & McPherson, T. N. (2009). Effect of land use-based surface roughness on hydrologic model output. *Journal of Spatial Hydrology*, *9*(2).

Kasmalkar, I., Wagenaar, D., Bill-Weilandt, A., Choong, J., Manimaran, S., Lim, T. N., et al. (2024). Flow-tub model: A modified bathtub flood model with hydraulic connectivity and path-based attenuation. *MethodsX*, *12*, 102524. https://doi.org/10.1016/j.mex.2023.102524

Knapp, K. R., Diamond, H. J., Kossin, J. P., Kruk, M. C., & Schreck, C. J. (2018). International best track archive for climate stewardship (IBTrACS) project, version 4 [Dataset]. https://doi.org/10.25921/82ty-9e16

Komurcu, M., Emanuel, K., Huber, M., & Acosta, R. (2018). High-resolution climate projections for the northeastern United States using dynamical downscaling at convection-permitting scales [Dataset]. *Earth and Space Science*, *5*(11), 801–826. https://doi.org/10.1029/2018EA000426

Kossin, J. P. (2018). A global slowdown of tropical-cyclone translation speed. *Nature*, *558*(7708), 104–107. https://doi.org/10.1038/s41586-018-0158-3

Kossin, J. P., Emanuel, K. A., & Vecchi, G. A. (2014). The poleward migration of the location of tropical cyclone maximum intensity. *Nature*, *509*(7500), 349–352. https://doi.org/10.1038/nature13278

Kulp, S. A., & Strauss, B. H. (2019). New elevation data triple estimates of global vulnerability to sea-level rise and coastal flooding. *Nature Communications*, *10*(1), 1–12. https://doi.org/10.1038/s41467-019-12808-z

Lin, N., Emanuel, K., Oppenheimer, M., & Vanmarcke, E. (2012). Physically based assessment of hurricane surge threat under climate change. *Nature Climate Change*, *2*(6), 462–467. https://doi.org/10.1038/nclimate1389

Lin, N., Kopp, R. E., Horton, B. P., & Donnelly, J. P. (2016). Hurricane Sandy's flood frequency increasing from year 1800 to 2100. *Proceedings of the National Academy of Sciences of the United States of America*, *113*(43), 12071–12075. https://doi.org/10.1073/pnas.1604386113

Lin, N., Marsooli, R., & Colle, B. A. (2019). Storm surge return levels induced by mid-to-late-twenty-first-century extratropical cyclones in the northeastern United States. *Climatic Change*, *154*(1–2), 143–158. https://doi.org/10.1007/s10584-019-02431-8

LISFLOOD developers. (2020). Lisflood-fp 8.0 hydrodynamic model (version 8.0) [Software]. *Zenodo*. https://doi.org/10.5281/zenodo.4073011

Little, C. M., Horton, R. M., Kopp, R. E., Oppenheimer, M., Vecchi, G. A., & Villarini, G. (2015). Joint projections of US East Coast sea level and storm surge. *Nature Climate Change*, *5*(12), 1114–1120. https://doi.org/10.1038/nclimate2801

Liu, M., Vecchi, G. A., Smith, J. A., & Knutson, T. R. (2019). Causes of large projected increases in hurricane precipitation rates with global warming. *NPJ Climate and Atmospheric Science*, *2*(1), 38. https://doi.org/10.1038/s41612-019-0095-3

Mandli, K. T., & Dawson, C. N. (2014). Adaptive mesh refinement for storm surge. *Ocean Modelling*, *75*, 36–50. https://doi.org/10.1016/j.ocemod.2014.01.002

Marsooli, R., Lin, N., Emanuel, K., & Feng, K. (2019). Climate change exacerbates hurricane flood hazards along US Atlantic and gulf coasts in spatially varying patterns. *Nature Communications*, *10*(1), 1–9. https://doi.org/10.1038/s41467-019-11755-z

Miura, Y., Mandli, K. T., & Deodatis, G. (2021). High-speed GIS-based simulation of storm surge–induced flooding accounting for sea level rise. *Natural Hazards Review*, *22*(3), 04021018. https://doi.org/10.1061/(asce)nh.1527-6996.0000465

Moftakhari, H. R., Salvadori, G., AghaKouchak, A., Sanders, B. F., & Matthew, R. A. (2017). Compounding effects of sea level rise and fluvial flooding. *Proceedings of the National Academy of Sciences of the United States of America*, *114*(37), 9785–9790. https://doi.org/10.1073/pnas.1620325114

Müller, M. (2011). Rapid change in semi-diurnal tides in the North Atlantic since 1980. *Geophysical Research Letters*, *38*(11), L11602. https://doi.org/10.1029/2011gl047312

National Centers for Environmental Information (NCEI). (2023). NOAA bathymetric data viewer [Dataset]. Retrieved from https://www.ncei.noaa.gov/maps/bathymetry/

National Oceanic and Atmospheric Administration (NOAA). (2023a). NOAA lidar data viewer [Dataset]. Retrieved from https://coast.noaa.gov/dataviewer/#/lidar/search/

National Oceanic and Atmospheric Administration (NOAA). (2023b). Sea level trends at station 8447930 [Dataset]. Retrieved from https://www.tidesandcurrents.noaa.gov/sltrends/sltrends_station.shtml?id=8447930

National Oceanic and Atmospheric Administration (NOAA). (2024). NEXRAD radar-based rainfall intensity data for station KBOX [Dataset]. Retrieved from https://www.ncdc.noaa.gov/nexradinv/chooseday.jsp?id=kbox

Neal, J., Schumann, G., & Bates, P. (2012). A subgrid channel model for simulating river hydraulics and floodplain inundation over large and data sparse areas. *Water Resources Research*, *48*(11), W11506. https://doi.org/10.1029/2012wr012514

Neumann, B., Vafeidis, A. T., Zimmermann, J., & Nicholls, R. J. (2015). Future coastal population growth and exposure to sea-level rise and coastal flooding-a global assessment. *PLoS One*, *10*(3), e0118571. https://doi.org/10.1371/journal.pone.0118571

Reed, A. J., Mann, M. E., Emanuel, K. A., Lin, N., Horton, B. P., Kemp, A. C., & Donnelly, J. P. (2015). Increased threat of tropical cyclones and coastal flooding to New York City during the anthropogenic era. *Proceedings of the National Academy of Sciences of the United States of America*, *112*(41), 12610–12615. https://doi.org/10.1073/pnas.1513127112

Roberts, K. J., Colle, B. A., & Korfe, N. (2017). Impact of simulated twenty-first-century changes in extratropical cyclones on coastal flooding at the battery, New York City. *Journal of Applied Meteorology and Climatology*, *56*(2), 415–432. https://doi.org/10.1175/jamc-d-16-0088.1

Sarhadi, A. (2024). Physics-based hazard assessment of compound flooding from tropical and extratropical cyclones in a warming climate [Dataset]. *Earth's Future*. Zenodo. https://doi.org/10.5281/zenodo.13732848

Sarhadi, A., Rousseau-Rizzi, R., Mandli, K., Neal, J., Wiper, M. P., Feldmann, M., & Emanuel, K. (2024). Climate change contributions to increasing compound flooding risk in New York City. *Bulletin of the American Meteorological Society*, *105*(2), E337–E356. https://doi.org/10.1175/bams-d-23-0177.1

Shepard, C. C., Agostini, V. N., Gilmer, B., Allen, T., Stone, J., Brooks, W., & Beck, M. W. (2012). Assessing future risk: Quantifying the effects of sea level rise on storm surge risk for the southern shores of long island, New York. *Natural Hazards*, *60*(2), 727–745. https://doi.org/10.1007/s11069-011-0046-8

Strauss, B. H., Orton, P. M., Bittermann, K., Buchanan, M. K., Gilford, D. M., Kopp, R. E., et al. (2021). Economic damages from hurricane sandy attributable to sea level rise caused by anthropogenic climate change. *Nature Communications*, *12*(1), 1–9. https://doi.org/10.1038/s41467-021-22838-1

Studholme, J., Fedorov, A. V., Gulev, S. K., Emanuel, K., & Hodges, K. (2022). Poleward expansion of tropical cyclone latitudes in warming climates. *Nature Geoscience*, *15*(1), 14–28. https://doi.org/10.1038/s41561-021-00859-1

United States Department of Agriculture (USDA). (2023). Soil available water storage [Dataset]. Retrieved from https://nrcs.app.box.com/v/soils/

United States Geological Survey (USGS). (2024). Flood level data for USGS gauge station 01105933 (December 27-29, 2012) [Dataset]. Retrieved from https://nwis.waterdata.usgs.gov/usa/nwis/uv/?cb_00065=on&format=gif_default&site_no=01105933&legacy=1&period=&begin_date=2012-12-27&end_date=2012-12-29

Wahl, T., Jain, S., Bender, J., Meyers, S. D., & Luther, M. E. (2015). Increasing risk of compound flooding from storm surge and rainfall for major US cities. *Nature Climate Change*, *5*(12), 1093–1097. https://doi.org/10.1038/nclimate2736

Westerink, J. J., Luettich, R. A., Feyen, J. C., Atkinson, J. H., Dawson, C., Roberts, H. J., et al. (2008). A basin-to channel-scale unstructured grid hurricane storm surge model applied to southern Louisiana. *Monthly Weather Review*, *136*(3), 833–864. https://doi.org/10.1175/2007mwr1946.1

Wickham, J., Stehman, S. V., Sorenson, D. G., Gass, L., & Dewitz, J. A. (2023). Thematic accuracy assessment of the NLCD 2019 land cover for the conterminous United States [Dataset]. *GIScience and Remote Sensing*, *60*(1). https://doi.org/10.1080/15481603.2023.2181143.2181143.

Wing, O. E., Lehman, W., Bates, P. D., Sampson, C. C., Quinn, N., Smith, A. M., et al. (2022). Inequitable patterns of us flood risk in the Anthropocene. *Nature Climate Change*, *12*(2), 156–162. https://doi.org/10.1038/s41558-021-01265-6

Xi, D., Lin, N., & Smith, J. (2020). Evaluation of a physics-based tropical cyclone rainfall model for risk assessment. *Journal of Hydrometeorology*, *21*(9), 2197–2218. https://doi.org/10.1175/jhm-d-20-0035.1

Zhang, Y., & Najafi, M. R. (2020). Probabilistic numerical modeling of compound flooding caused by tropical storm Matthew over a data-scarce coastal environment. *Water Resources Research*, *56*(10), e2020WR028565. https://doi.org/10.1029/2020wr028565